technology. We found that gene expressions of cyclin-dependent kinase inhibitor 1A (CDKI1A) and mitogen-activated protein kinase phosphatase-1 (MKP-1), but not growth factors, are induced in chronic pressure-overloaded atrial myocardium. These results suggest that suppressors of the cell cycle or cell proliferation may play a critical role in the pathophysiology of pressure overload.

2. Methods

2.1. Materials

Fibronectin, fetal calf serum, and Hanks' balanced salt solution were purchased from Life Technologies (Rockville, MD). All other chemicals were purchased from Sigma (St. Louis, MO).

2.2. Subjects

This study group consisted of five men and four women (mean age 59 ± 19 years) who underwent cardiac surgery. Hemodynamic studies were performed the morning after an overnight fast. Vasodilators were withheld for at least 24 h before evaluation. Chronic, stable doses of digoxin and diuretics were continued but were administered on an evening schedule. Right and left heart studies, including measurement of pressure, biplane left ventriculography and coronary angiography, were performed using a percutaneous cathether. The severity of tricuspid regurgitation was estimated by color Doppler echocardiography with a 2.5-MHz transducer (SONOS 2500 system, Hewlett Packard, Palo Alto, CA). The severity of tricuspid regurgitation was graded on a four-point scale, based on the distance reached by the abnormal signals from the tricuspid orifice toward the posterior wall in the parasternal four-chamber view [11]. Tricuspid regurgitation was classified as trivial, mild, moderate, or severe. This study was approved by our institutional human investigations committee, and written informed consent was obtained from all patients before participation.

2.3. Atrial myocardium samples

Right atrial appendages were obtained from the patients during cardiac surgery. Pieces of right atrial appendage weighing 200–1400 mg were frozen immediately in liquid nitrogen and stored at −80 °C.

2.4. Transcriptional profiling

Total RNA was isolated by the guanidinium thiocyanate and phenol chloroform method [12]. Preparation of biotin-labeled cRNA probes were performed with the following steps; conversion of RNA to single strand cDNA by reverse transcriptase reactions and synthesis of double strand cDNA template using SuperScript II kit (Life Technologies), purification of double-strand cDNA template using QIAquick PCR purification kit (QIAGEN, Valencia, CA), and transcription of biotin-labeled cRNA (AmpliScribe kit, Epicentre Technologies, Madison, WI) according to the manufacturer's instructions. The DNA microarray hybridization of biotin-labeled cRNA was performed using ExpressChip HO1 and HO2 arrays (Mergen, San Leandro, CA) according to the manufacturer's instructions. The ExpressChip HO1 and HO2 arrays have 2139 well-characterized genes with putative functions. A complete listing of genes contained within ExpressChip HO1 and HO2 can be found at http://www.mergen-ltd.com/HO1/HO1abc_genelist.htm and http://www.mergen-ltd.com/HO2/HO2abc_genelist.htm. The chips were subjected to the laser scanning and signal detection by the GMS418 Array Scanner (Takara Biomedicals, Shiga, Japan). The intensity of emission signals in each oligonucleotide hybridization was normalized to that of the glyceraldehyde-3 phosphate dehydrogenase (GAPDH) signal and analyzed using the GeneSpring software package (Silicon Genetics, Redwood City, CA).

2.5. Real-time reverse transcription–polymerase chain reaction (PCR) analysis

For reverse transcription, RNA was reverse transcribed using T7-dT primer (5′ -TCT AGT CGA CGG CCA GTG AAT TGT AAT ACG ACT CAC TAT AGG GCG TTT TTT TTT TTT TTT TTT TTT-3′) and Superscript II reverse transcriptase (Life Technologies). Real-time quantitative PCR was performed in optical tubes in a 96-well microtiter plate (Perkin-Elmer/Applied Biosystems, Foster City, CA) with an ABI PRISM 7700 Sequence Detector Systems (Perkin-Elmer/Applied Biosystems) according to the manufacturer's instructions. By using the SYBR Green PCR Core Reagents Kit (Perkin-Elmer/Applied Biosystems, P/N 4304886), fluorescence signals were generated during each PCR cycle via the 5′ - to 3′ - endonuclease activity of Taq Gold [13] to provide real-time quantitative PCR information. The oligonucleotide primers used for real-time PCR analysis were shown in Table 1. No template controls as well as the samples were added in a total volume of 50 μl/reaction. Potential PCR product contamination was digested by uracil-*N*-glycosylase, because dTTP is substituted by dUTP [13]. All PCR experiments were performed with the hot start method. In the reaction system, uracil-*N*-glycosylase and Taq Gold (Perkin-Elmer/Applied Biosystems) were applied according to the manufacturer's instructions [13,14]. Denaturing and annealing reactions were performed 40 times at 95 °C for 15 s, and at 60 °C for CDKI1A, 54 °C for MKP-1, 56 °C for glutathione S-transferase theta 1 and 62 °C

Table 1
Design of primers for real-time PCR

Gene		Primer sequences	PCR product (bp)
CDKI1A	Sense	5′ -GACCTGTCACTGTCTTGTACCCTT-3′	120
	Antisense	5′ -GTAGAAATCTGTCATGCTGGTCTG-3′	
MKP-1	Sense	5′ -TTTTGAGGGTCACTACCAGTACAA-3′	191
	Antisense	5′ -TAGTCCTCATAAGGTAAGCAAGGC-3′	
GSTT1	Sense	5′ -GTAGCCATCACGGAGCTGAT-3′	146
	Antisense	5′ -CTTGGCCTTCAGAATGACCT-3′	
SCYA5	Sense	5′ -AAGGAGTATTTCTACACCAGTGGC-3′	132
	Antisense	5′ -GCTCATCTCCAAAGAGTTGATGTA-3′	

CDKI1A, cyclin-dependent kinase inhibitor 1A; GSTT1, glutathione S-transferase theta 1; MKP-1, mitogen-activated protein kinase phosphatase-1; SCYA5, small inducible cytokine A5.

for small inducible cytokine A5 for 1 min, respectively. The increase in the fluorescence signal is proportional to the amount of specific product [15]. The intensity of emission signals in each sample was normalized to that of β-actin as an internal control.

2.6. Culture of neonatal rat ventricular myocytes (NRVM)

NRVM from 1-day-old Sprague–Dawley rats were isolated by previously described methods [16]. The ventricles were excised from the rat, cut into several pieces, and incubated overnight at 4 °C in 1 mg/ml of 1:300 trypsin in Hanks' balanced salt solution. The ventricular tissue was then digested with 1 mg/ml of collagenase type II (239 U/mg, Worthington Biochemicals, Freehold, NJ) in Hanks' balanced salt solution, centrifuged twice at $50 \times g$ to remove less dense cells such fibroblasts, and then plated. The cells were cultured at 37 °C, 5% CO_2 in Dulbecco's modified Eagle's medium (BioWhittaker, Walkersville, MD) containing 7% fetal calf serum, 50 U/ml penicillin and 50 μg/ml streptomycin. We routinely obtained primary cultures with >95% myocytes, as assessed by microscopic observation of spontaneous contraction and by immunofluorescence staining with a monoclonal human ventricular myosin heavy chain antibody (Biogenesis, Poole, UK) [16].

This investigation was performed according to the *Guide for the Care and Use of Laboratory Animals* published by US National Institutes of Health (NIH publication No. 85-23, revised 1996).

2.7. Mechanical strain device and preparation of cells

Mechanical deformation was applied to a thin and transparent membrane on which cells were cultured, an approach which produces controlled cellular strain as well as visualization of cells [17].

For the preparation of NRVM to be subjected to mechanical strain, autoclaved membrane dishes were coated with 2 μg/ml of fibronectin in 13 ml of Hanks' balanced salt solution for 6–12 h at 4 °C and then washed twice with 10 ml of phosphate-buffered saline. NRVM were plated on the coated membrane dish at a density of 2,000,000 cells/dish in 13 ml of Dulbecco's modified Eagle's medium containing 7% fetal calf serum and incubated 48 h. NRVM were then made quiescent by washing with 10 ml of Hanks' balanced salt solution twice and incubating with 10 ml of Dulbecco's modified Eagle's medium containing 1% insulin, transferrin, selenium media supplement (ITS; Sigma), 50 U/ml penicillin, and 50 μg/ml streptomycin. All experiments were performed on NRVM that had been serum-starved for 24 h.

2.8. Western analysis

NRVM were lysed directly in each dish by application of a buffer containing 50 mM Tris–HCl (pH 7.5), 1 mM EDTA, 1 μM leupeptin, 1 μM pepstatin A, 0.1 mM phenylmethylsulfonyl fluoride, and 1 mM dithiothreitol, and sonicated. The homogenates were then centrifuged at $100{,}000 \times g$ for 20 min. Total protein concentration was measured by the Bradford method (Bio-Rad Laboratories, Hercules, CA) and equal quantities of total protein were loaded on a 13% SDS–polyacrylamide gel and transferred to a nitrocellulose membrane in 25 mM Tris base (pH 8.5), 0.2 M glycine, and 20% methanol. The nitrocellulose membrane was blocked by 5% non fat dried milk in Tris-buffered saline washing buffer containing 20 mM Tris base (pH 7.6), 137 mM NaCl, and 0.1% Tween 20 for 2 h. For the detection of CDKI1A and MKP-1, the membrane was incubated with 1:1000 diluted mouse monoclonal anti-CDKI1A antibody (sc-6246, Santa Cruz Biotechnology, Santa Cruz, CA) or rabbit polyclonal anti-MKP-1 antibody (sc-1199, Santa Cruz Biotechnology) for 1 h at 37 °C and washed with Tris-buffered saline washing buffer for 30 min. After application of sheep anti-mouse IgG (Amersham Life Science, Arlington Heights, IL) or goat anti-rabbit IgG (Santa Cruz Biotechnology) coupled to peroxidase, the membrane was developed with the enhanced chemiluminescent method (Amersham Life Science).

Table 2
Patient characteristics

Patient (no.)	Age (years)	Sex	Diagnosis	mRAP (mm Hg)	Systolic PAP (mm Hg)	TR grade
Control						
1	44	M	AR	3	19	trivial
2	70	F	MR	4	28	trivial
3	60	M	AS	6	34	trivial
Pressure overload						
1	64	M	MR	10	52	mild
2	74	F	MR, AS	15	65	mild
3	75	M	MR, AR	8	53	mild
Volume overload						
1	64	F	MR	4	32	moderate
2	64	F	AR, MR	5	32	severe
3	15	M	ASD	5	23	moderate

AR, aortic regurgitation; AS, aortic stenosis; ASD, atrial septal defect; F, female; M, male; MR, mitral regurgitation; mRAP, mean right atrial pressure; PAP, pulmonary artery pressure; TR, tricuspid regurgitation.

2.9. Statistical analysis

Data are expressed as mean ± S.D. The data were analyzed by nonparametric Kruskal–Wallis methods for the group comparisons to avoid assumptions about the distribution of the measured variables. Subsequent pairwise comparisons were made with the Mann–Whitney *U* test. A *P* value <0.05 was considered significant.

3. Results

3.1. Clinical characteristics of participating subjects

On the basis of pressure data of Swan–Ganz catheters and echocardiographic findings, the patients were divided into the following three groups: control group ($n=3$), pressure overload group (mean right atrial pressure of >7 mm Hg, $n=3$), and volume overload group (moderate or severe tricuspid regurgitation, $n=3$) (Table 2).

3.2. DNA microarray analysis

Among the 2139 well-characterized genes with putative functions, expression of genes of CDKI1A (11.7 ± 3.1-fold vs. control), MKP-1 (26.2 ± 2.1-fold), glutathione S-transferase theta 1 (65.1 ± 29.7-fold) and small inducible cytokine A5 (8.3 ± 1.8-fold) in the pressure overload group significantly increased compared with those in control ($P<0.05$) or volume overload group (CDKI1A, 3.0 ± 2.0-fold vs. control; MKP-1, 8.1 ± 6.5-fold; glutathione S-transferase theta 1, 19.2 ± 10.1-fold; small inducible cytokine A5, 2.1 ± 0.7-fold, $P<0.05$), as shown in Fig. 1. In contrast, transcripts of growth factors such as fibroblast growth factor, hepatocyte growth factor, insulin-like growth factor, platelet-derived growth factor and vascular endothelial growth factor, and cytokines including interleukin 1,

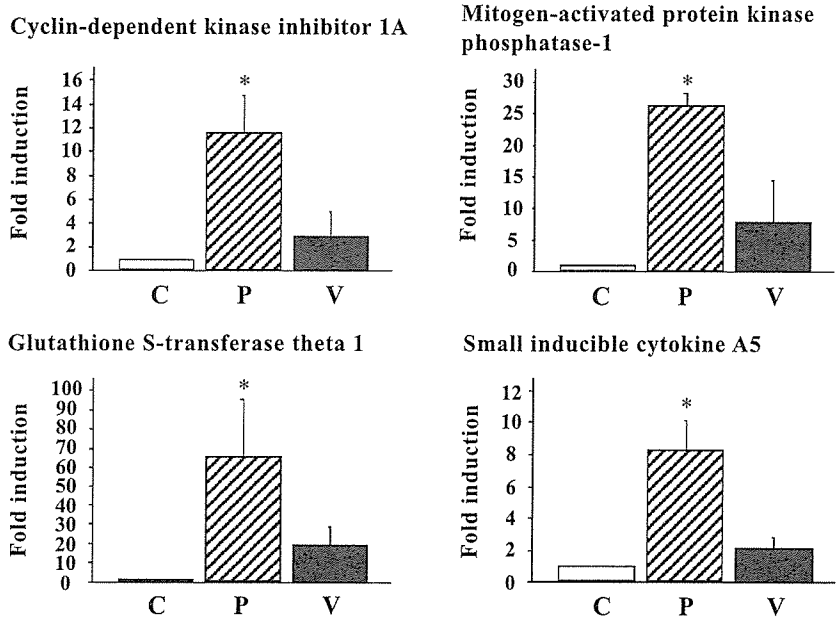

Fig. 1. Oligonucleotide microarray analysis of pressure- or volume-overloaded human myocardium. Total RNA was obtained from the right atrial appendages of the patients: control group (C, open bar), pressure overload group (P, hatched bar), and volume overload group (V, closed bar). Preparation of biotin-labeled cRNA probes was performed as described in the Methods. The DNA microarray hybridization of biotin-labeled cRNA was performed using ExpressChip HO1 and HO2 arrays (Mergen). The chips were subjected to the laser scanning and signal detection by the GMS418 Array Scanner (Takara Biomedicals). The intensity of emission signals in each oligonucleotide hybridization was normalized to that of the glyceraldehyde-3 phosphate dehydrogenase signal, and analyzed using the GeneSpring software package (Silicon Genetics). The mRNA expression was expressed as relative change standardized to control group. Bar graphs with error bars represent the mean ± S.D. ($n=3$). *$P<0.05$ vs. control or volume overload group.

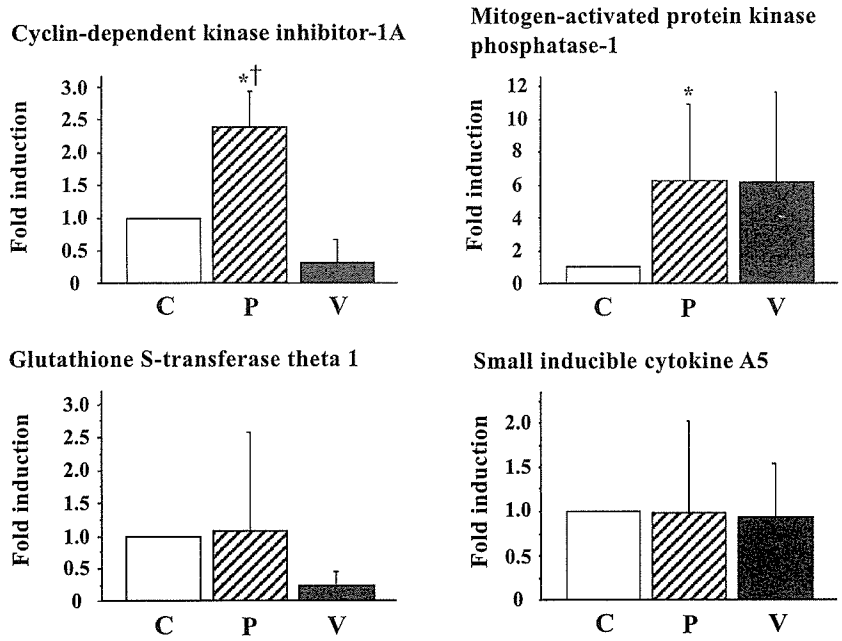

Fig. 2. Quantitative real-time reverse transcription–PCR analysis. The cDNA was prepared from the right atrial appendages of the patients: control group (C, open bar), pressure overload group (P, hatched bar), and volume overload group (V, closed bar), and then subjected to real-time PCR with primers specific for cyclin-dependent kinase inhibitor 1A, mitogen-activated protein kinase phosphatase-1, glutathione S-transferase theta 1, small inducible cytokine A5 or β-actin. The ratio of the abundance of each transcript to that of the β-actin transcript was calculated, and the amount of mRNA expression was expressed as relative change standardized to control group. Bar graphs with error bars represent the mean ± S.D. ($n=3$). *$P<0.05$ vs. control. †$P<0.05$ vs. volume overload group.

interleukin 6, interleukin 8, and tumor necrosis factor α were not significantly different among the three groups.

3.3. Quantitation of the selected genes by real-time PCR

To confirm the preferential expression of the selected genes in pressure overload group, we prepared cDNAs from the same RNA as that used in microarray analysis, and then subjected these cDNAs to "real-time" PCR analysis with primers specific for CDKI1A, MKP-1, glutathione S-transferase theta 1, small inducible cytokine A5 and β-actin (Fig. 2). The abundance of CDKI1A (2.4 ± 0.5-fold vs. control) mRNA relative to that of β-actin mRNA in pressure overload group was markedly greater than that in control ($P<0.05$) or volume overload group (0.3 ± 0.4-fold, $P<0.05$). The abundance of MKP-1 (6.2 ± 4.7-fold) mRNA relative to that of β-actin mRNA in pressure overload group was significantly greater than that in control ($P<0.05$), but not in volume overload group (6.2 ± 5.5-fold). However, the abundance of glutathione S-transferase theta 1 and small inducible cytokine A5 mRNA was not significant different among three groups (glutathione S-transferase theta 1: pressure overload group, 1.1 ± 1.5-fold vs. control; volume overload group, 0.3 ± 0.2-fold and small inducible cytokine A5: pressure overload group, 1.0 ± 1.0-fold vs. control; volume overload group, 0.9 ± 0.6-fold). Thus, these findings demonstrated that gene expressions of CDKI1A and MKP-1 are increased in the human atrial myocardium with pressure overload.

3.4. Effects of mechanical strain on CDKI1A and MKP-1 protein accumulation

Next, we investigated whether CDKI1A and MKP-1 proteins were induced by mechanical strain in cardiac myocytes. The expressions of CDKI1A and MKP-1 proteins were analyzed by immunoblotting with anti-CDKI1A and MKP-1 antibodies, respectively. As shown in Fig. 3, mechanical strain at a frequency of 1 Hz induced CDKI1A and MKP-1 protein expressions in an amplitude-dependent manner.

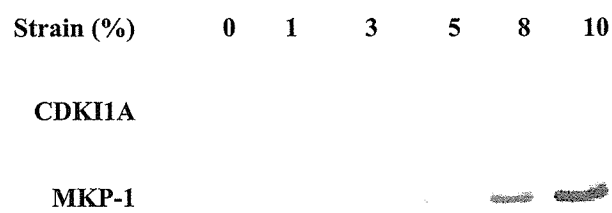

Fig. 3. Effects of mechanical strain on cyclin-dependent kinase inhibitor 1A (CDKI1A) and mitogen-activated protein kinase phosphatase-1 (MKP-1) protein expressions in cardiac myocytes. Cardiac myocytes were plated on 2 μg/ml of fibronectin in Dulbecco's modified Eagle's medium containing 7% fetal calf serum for 24 h. After serum deprivation for 24 h, myocytes were exposed to 0%, 1%, 3%, 5%, 8%, or 10% cyclic mechanical strain (1 Hz) for 2 h. Cell extracts were subjected to SDS–PAGE followed by immunoblot analysis using the anti-CDKI1A or MKP-1 antibody. Data are representative of two independent experiments with nearly identical results.

4. Discussion

Most previous studies have focused on the activation of pathways of signal transduction in the cardiac hypertrophy or remodeling. In the present study, gene expressions of CDKI1A and MKP-1, but not growth factors, were induced in chronic pressure-overloaded myocardium. In addition, mechanical strain induced CDKI1A and MKP-1 at a protein level in cultured rat cardiac myocytes in an amplitude-dependent manner. These findings suggest that negative regulators of cell cycle or cell proliferation also may play an important role in the pathophysiology of pressure overload.

Relatively little is known about the molecular changes associated with volume-overload hypertrophy. Lattion et al. [18] reported that aortocaval fistula in rat caused a highly significant increase in atrial natriuretic factor gene expression in the left ventricle. In addition, Calderone et al. [19] reported that pressure overload, but not volume overload, increased mRNA levels for β-myosin heavy chain and skeletal α-actin in rats, while both pressure overload and volume overload caused comparable increases in left ventricular weight. Our results also demonstrated that there are molecular differences between pressure- and volume-overloaded myocardium.

Many intracellular signaling pathways are thought to play important roles in mechanotransduction. Recent studies of myocardial hypertrophy have focused on activation of protein kinases including protein kinase C, Raf-1 kinase, S6 peptide kinase and mitogen-activated protein (MAP) kinases, which precede an increase in specific gene expression and protein synthesis [20–22]. The MAP kinase signaling pathways consist of three major phosphorylation cascades: the extracellular signaling-regulated protein kinases, the c-Jun NH_2-terminal kinases, and the p38-MAP kinases [23]. MKP-1 has dual catalytic activity toward phosphotyrosine- and phosphothreonine-containing proteins and is known to inactivate extracellular signaling-regulated protein kinases, possibly c-Jun NH_2-terminal kinases and p38-MAP kinases [24–27]. MKP-1 is an important member of the dual specificity phosphatase family that is expressed in the heart. Transient transfection of an MKP-1-encoding expression vector into cardiac myocytes was shown to downregulate multiple hypertrophy-induced promoter constructs in vitro [28,29]. Recently, Bueno et al. [30] reported that transgenic mice constitutively expressing MKP-1 in the heart showed attenuation in normal developmental hypertrophy and concomitant ventricular dilation, and demonstrated that adult MKP-1 transgenic mice failed to mount a significant hypertrophic response when stressed by pressure overload or isoproterenol infusion. Interestingly, in the present study, MKP-1 mRNA and protein expressions were induced in chronic human pressure-overloaded myocardium and mechanically stimulated cardiac myocytes, respectively. Taken together, these findings suggest that MKP-1 as well as MAP kinase pathway may be a critical regulator of cardiac hypertrophy or remodeling.

Cyclin/cyclin-dependent kinase complexes facilitate progression through the cell cycle and are activated at specific points during the cell cycle [31]. CDKI1A (also named WAF1, and CIP1), p21, is involved in regulating cell cycle progression. CDKI1A, which functions by binding to and inactivating a number of the cyclin/cyclin-dependent kinase complexes including cyclin-dependent kinase 2, is a regulator of the G_1–S cell cycle checkpoint. Poolman and Brooks [32] reported that CDKI1A is induced during the 2–5-day developmental period in rat cardiac myocytes. The induction and sustained expression of CDKI1A is considered to be a contributory mechanism by which myocytes irreversibly exit the cell cycle upon terminal differentiation [33]. However, cell cycle in adult cardiac myocytes, particularly when stimulated by hypertrophic stimuli, remains fully undefined. Recently, Liao et al. [34] demonstrated that cardiac overexpression of cyclin-dependent kinase 2 resulted in increased numbers of smaller, less-differentiated mononuclear cardiac myocytes in adult hearts, and that surgically induced pressure overload caused an exaggerated maladaptive hypertrophic response in transgenic mice. Beltrami et al. [35] reported that a subpopulation of human adult myocytes evidently reentered the cell cycle and underwent nuclear mitotic division early after myocardial infarction. The present study demonstrated that CDKI1A mRNA expression was induced in chronic human pressure-overloaded myocardium and that CDKI1A protein expression was induced by mechanical strain in cardiac myocytes in an amplitude-dependent manner. Therefore, it is likely that the mechanism of cell cycle withdrawal is not irreversible in cardiac myocytes.

4.1. Study limitations

The number of patients in this study was small and might not be representative for conditions investigated. In addition, we used the atrial samples, because it is very difficult to obtain human left ventricles.

A greater understanding of the cell cycle or cell proliferation that is related to cardiac hypertrophy or remodeling will be critical for implementing novel and more effective therapeutic strategies in the future. However, the mechanism of cell cycle or cell proliferation in cardiac myocytes, particularly adult cardiac myocytes, is complicated and poorly understood. The present study demonstrates that gene expressions of CDKI1A and MKP-1, but not growth factors, are induced in chronic pressure-overloaded myocardium and suggests that suppressors of cell cycle or cell proliferation may modulate the pathophysiology of pressure overload. Furthermore, additional studies are needed to clarify the mechanism of cell cycle or cell proliferation in the heart.

Acknowledgements

This study was supported by grants from the Ministry of Education, Science, Sports and Culture of Japan

(12670686), Tokyo, Japan, the Kanae Foundation for Life and Socio-Medical Science, Tokyo, Japan and the Mitsui Life Social Welfare Foundation, Tokyo, Japan.

References

[1] Levy D, Garrison RJ, Savage DD, Kannel WB, Castelli WP. Prognostic implications of echocardiographically determined left ventricular mass in the Framingham Heart Study. N Engl J Med 1990;322:1561–6.

[2] Anversa P, Olivetti G, Melissari M, Loud AV. Stereological measurement of cellular and subcellular hypertrophy and hyperplasia in the papillary muscle of adult rat. J Mol Cell Cardiol 1980;12:781–95.

[3] Morkin E. Postnatal muscle fiber assembly: localization of newly synthesized myofibrillar proteins. Science 1970;167:1499–501.

[4] Anversa P, Levicky V, Beghi C, McDonald SL, Kikkawa Y. Morphometry of exercise-induced right ventricular hypertrophy in the rat. Circ Res 1983;52:57–64.

[5] Gerdes AM, Campbell SE, Hilbelink DR. Structural remodeling of cardiac myocytes in rats with arteriovenous fistulas. Lab Invest 1988;59:857–61.

[6] Yamamoto K, Dang QN, Maeda Y, Huang H, Kelly RA, Lee RT. Regulation of cardiomyocyte mechanotransduction by the cardiac cycle. Circulation 2001;103:1459–64.

[7] Schena M, Shalon D, Davis RW, Brown PO. Quantitative monitoring of gene expression patterns with a complementary DNA microarray. Science 1995;270:467–70.

[8] Shalon D, Smith SJ, Brown PO. A DNA microarray system for analyzing complex DNA samples using two-color fluorescent probe hybridization. Genome Res 1996;6:639–45.

[9] Iyer VR, Eisen MB, Ross DT, et al. The transcriptional program in the response of human fibroblasts to serum. Science 1999;283:83–7.

[10] Feng Y, Yang JH, Huang H, et al. Transcriptional profile of mechanically induced genes in human vascular smooth muscle cells. Circ Res 1999;85:1118–23.

[11] Miyatake K, Okamoto M, Kinoshita N, et al. Evaluation of tricuspid regurgitation by pulsed Doppler and two-dimensional echocardiography. Circulation 1982;66:777–89.

[12] Chomczynski P, Sacchi N. Single-step method of RNA isolation by acid guanidinium thiocyanate–phenol–chloroform extraction. Anal Biochem 1987;162:156–9.

[13] Heid CA, Stevens J, Livak KJ, Williams PM. Real time quantitative PCR. Genome Res 1996;6:986–94.

[14] Kruse N, Pette M, Toyka K, Rieckmann P. Quantification of cytokine mRNA expression by RT PCR in samples of previously frozen blood. J Immunol Methods 1997;210:195–203.

[15] Lockhart DJ, Dong H, Byrne MC, et al. Expression monitoring by hybridization to high-density oligonucleotide arrays. Nat Biotechnol 1996;14:1675–80.

[16] Yamamoto K, Dang QN, Kennedy SP, Osathanondh R, Kelly RA, Lee RT. Induction of tenascin-C in cardiac myocytes by mechanical deformation: role of reactive oxygen species. J Biol Chem 1999;274:21840–6.

[17] Cheng GC, Briggs WH, Gerson DS, et al. Mechanical strain tightly controls fibroblast growth factor-2 release from cultured human vascular smooth muscle cells. Circ Res 1997;80:28–36.

[18] Lattion AL, Michel JB, Arnauld E, Corvol P, Soubrier F. Myocardial recruitment during ANF mRNA increase with volume overload in the rat. Am J Physiol 1986;251:H890–6.

[19] Calderone A, Takahashi N, Izzo Jr NJ, Thaik CM, Colucci WS. Pressure- and volume-induced left ventricular hypertrophies are associated with distinct myocyte phenotypes and differential induction of peptide growth factor mRNAs. Circulation 1995;92:2385–90.

[20] Komuro I, Katoh Y, Kaida T, et al. Mechanical loading stimulates cell hypertrophy and specific gene expression in cultured rat cardiac myocytes. Possible role of protein kinase C activation. J Biol Chem 1991;266:1265–8.

[21] Yamazaki T, Tobe K, Hoh E, et al. Mechanical loading activates mitogen-activated protein kinase and S6 peptide kinase in cultured rat cardiac myocytes. J Biol Chem 1993;268:12069–76.

[22] Sadoshima J, Izumo S. Mechanical stretch rapidly activates multiple signal transduction pathways in cardiac myocytes: potential involvement of an autocrine/paracrine mechanism. EMBO J 1993;12:1681–92.

[23] Hunter T. Oncoprotein networks. Cell 1997;88:333–46.

[24] Sun H, Tonks NK, Bar-Sagi D. Inhibition of Ras-induced DNA synthesis by expression of the phosphatase MKP-1. Science 1994;266:285–8.

[25] Misra-Press A, Rim CS, Yao H, Roberson MS, Stork PJ. A novel mitogen-activated protein kinase phosphatase. Structure, expression, and regulation. J Biol Chem 1995;270:14587–96.

[26] Liu Y, Gorospe M, Yang C, Holbrook NJ. Role of mitogen-activated protein kinase phosphatase during the cellular response to genotoxic stress: inhibition of c-Jun N-terminal kinase activity and AP-1-dependent gene activation. J Biol Chem 1995;270:8377–80.

[27] Lai K, Wang H, Lee WS, Jain MK, Lee ME, Haber E. Mitogen-activated protein kinase phosphatase-1 in rat arterial smooth muscle cell proliferation. J Clin Invest 1996;98:1560–7.

[28] Thorburn J, Carlson M, Mansour SJ, Chien KR, Ahn NG, Thorburn A. Inhibition of a signaling pathway in cardiac muscle cells by active mitogen-activated protein kinase kinase. Mol Biol Cell 1995;6:1479–90.

[29] Fuller SJ, Davies EL, Gillespie-Brown J, Sun H, Tonks NK. Mitogen-activated protein kinase phosphatase 1 inhibits the stimulation of gene expression by hypertrophic agonists in cardiac myocytes. Biochem J 1997;323:313–9.

[30] Bueno OF, De Windt LJ, Lim HW, et al. The dual-specificity phosphatase MKP-1 limits the cardiac hypertrophic response in vitro and in vivo. Circ Res 2001;88:88–96.

[31] Sherr CJ. G1 phase progression: cycling on cue. Cell 1994;79:551–5.

[32] Poolman RA, Brooks G. Expressions and activities of cell cycle regulatory molecules during the transition from myocyte hyperplasia to hypertrophy. J Mol Cell Cardiol 1998;30:2121–35.

[33] Guo K, Wang J, Andres V, Smith RC, Walsh K. MyoD-induced expression of p21 inhibits cyclin-dependent kinase activity upon myocyte terminal differentiation. Mol Cell Biol 1995;15:3823–9.

[34] Liao HS, Kang PM, Nagashima H, et al. Cardiac-specific overexpression of cyclin-dependent kinase 2 increases smaller mononuclear cardiomyocytes. Circ Res 2001;88:443–50.

[35] Beltrami AP, Urbanek K, Kajstura J, et al. Evidence that human cardiac myocytes divide after myocardial infarction. N Engl J Med 2001;344:1750–7.

Cancer Chemother Pharmacol (2004) 54: 505–513
DOI 10.1007/s00280-004-0839-5

ORIGINAL ARTICLE

Yasuhiko Kano · Miyuki Akutsu · Saburo Tsunoda
Tohru Izumi · Kiyoshi Mori · Hirofumi Fujii
Yasuo Yazawa · Hiroyuki Mano · Yusuke Furukawa

Schedule-dependent synergism and antagonism between pemetrexed and paclitaxel in human carcinoma cell lines in vitro

Received: 4 August 2003 / Accepted: 24 March 2004 / Published online: 31 August 2004

Abstract Pemetrexed is a novel multitargeted antifolate with significant clinical activity against a variety of tumors. We studied the schedule-dependent cytotoxic effects of pemetrexed in combination with paclitaxel in vitro to improve our understanding of how this combination might be used clinically. Human lung cancer A549 cells, breast cancer MCF7, ovarian cancer PA1, and colon cancer WiDr cells were exposed to both pemetrexed and paclitaxel in vitro. Cell growth inhibition after 5 days was determined and the effects of drug combinations were analyzed by the isobologram method (Steel and Peckham). Simultaneous exposure to pemetrexed and paclitaxel for 24 h produced antagonistic effects in A549 and PA1 cells, additive/antagonistic effects in MCF7 cells, and additive effects in WiDr cells. Pemetrexed for 24 h followed by paclitaxel for 24 h produced synergistic effects in A549 and MCF7 cells and additive effects in PA1 and WiDr cells, while the reverse sequence produced additive effects in all four cell lines. Cell cycle analysis supported these observations. Our findings suggest that the simultaneous administration of pemetrexed and paclitaxel is suboptimal. The optimal schedule of pemetrexed in combination with paclitaxel is the sequential administration of pemetrexed followed by paclitaxel, and this schedule should be assessed in clinical trials for the treatment of solid tumors.

Y. Kano (✉) · M. Akutsu · S. Tsunoda · T. Izumi
Division of Hematology, Tochigi Cancer Center,
Yonan, Utsunomiya, Tochigi, 320-0834, Japan
E-mail: ykano@tcc.pref.tochigi.jp
Tel.: +81-28-6585151
Fax: +81-28-6585488

K. Mori · H. Fujii
Division of Medical Oncology, Tochigi Cancer Center,
Utsunomiya, Tochigi, Japan

Y. Yazawa
Division of Orthopedic Oncology, Tochigi Cancer Center,
Utsunomiya, Tochigi, Japan

H. Mano · Y. Furukawa
Center for Molecular Medicine, Department of Hematology,
Jichi Medical School, Minamikawachi, Tochigi, Japan

Keywords Pemetrexed · Paclitaxel · Isobologram · Synergism · Antagonism

Introduction

The development of several new antifolates with distinctive chemical features and target enzymes has provided new opportunities to expand the role of antifolates in cancer chemotherapy. Multitargeted antifolate (MTA, pemetrexed) is a pyrrole-pyrimidine analogue of folate [33] currently in broad clinical evaluation. Pemetrexed is transported into cells mainly through the reduced folate carrier system and metabolized to polyglutamated forms [7] which inhibit thymidylate synthase, dihydrofolate reductase, and glycinamide ribonucleotide formyl transferase [30, 31], and has antithymidylate and antipurine effects [5]. Preclinical studies of pemetrexed have demonstrated its antitumor activity against a variety of human cancer cells [2, 29].

Phase I studies have shown that the dose-limiting toxicity includes neutropenia and thrombocytopenia, and other toxicities which are manageable, such as mucositis, skin rashes and transient elevations of transaminases [18, 23–25]. Daily and weekly schedules are associated with severe toxicity and 500 mg/m^2 of pemetrexed every 3 weeks was selected as the optimal schedule and dose for the further development of pemetrexed. Patients with a folate-deficient state showed severe toxicity. In preclinical models, folate supplementation reduced toxicity while maintaining antitumor activity. Based on these observations, folate and cobalamin administration before pemetrexed has been routine in recent clinical trials of pemetrexed [9, 26]. Pharmacokinetic studies have shown that pemetrexed undergoes biphasic plasma clearance with a terminal half-life of 1.1–3.1 h, depending on the schedule of administration [23]. The findings from the phase II trial results are encouraging: clear responses were observed in colorectal cancer, pancreatic cancer, lung cancer, breast cancer, mesothelioma, etc. [3, 4, 8, 10, 19–21, 26, 37]. A recent

phase III study has shown that treatment with pemetrexed and cisplatin results in survival times superior to those achieved with cisplatin alone in patients with malignant pleural mesothelioma [39].

Paclitaxel is an established anticancer agent with activity against a variety of solid tumors [1, 6]. Paclitaxel is a mitotic inhibitor that promotes the polymerization and stabilization of tubulin to microtubules [27]. Clinical studies have indicated that neutropenia is the dose-limiting toxicity of paclitaxel [1, 6]. Other toxicities include hypersensitivity reactions, neurotoxicity, mucositis, mild nausea and vomiting, and cardiac injury.

The combination of pemetrexed and paclitaxel may have a major role in the treatment of a variety of solid tumors. The wide range of antitumor activity of pemetrexed and paclitaxel, their different cytotoxic mechanisms and toxic profiles, and the absence of cross-resistance, provide the rationale for using combinations of these agents. Since pemetrexed and paclitaxel are cell cycle-specific agents [17, 38], the disturbances of the cell cycle produced by these agents may influence the cytotoxic effects of each agent, and the drug schedule may play a significant role in the outcome. Therefore, the design of a protocol using them in combination requires careful consideration. As expected, experimental studies for the combination of pemetrexed [22, 30, 36] or paclitaxel [13–15] with other agents have shown schedule-dependent interactions.

The aim of the present study was to elucidate the cytotoxic effects of combinations of pemetrexed and paclitaxel in various schedules on four human carcinoma cell lines. The data obtained were analyzed using the isobologram method of Steel and Peckham [32]. The combination showed schedule-dependent synergism and antagonism.

Materials and methods

Cell lines

Experiments were conducted with the human lung cancer A549, breast cancer MCF7, ovarian cancer PA1, and colon cancer WiDr cell lines. These cells were obtained from the American Type Culture Collection (Rockville, Md.) and maintained in 75-cm^2 plastic tissue culture flasks containing RPMI-1640 medium (Sigma Chemical Co., St Louis, Mo.) supplemented with 10% heat-inactivated fetal bovine serum (FBS) (Grand Island Biological Co.) and antibiotics. The cells used were devoid of mycoplasma infection. The doubling times of A549, MCF7, PA1, and WiDr cells under our experimental conditions were in the range 20–24 h.

Drugs

Pemetrexed was kindly provided by Eli Lilly and Company (Indianapolis, Ind.). Paclitaxel was purchased from Bristol-Myers Squibb Japan Co. (Tokyo). The drugs, at a concentration of 1 m*M*, were stored at −20°C and diluted with RPMI-1640 plus 10% FBS prior to use.

Cell growth inhibition using combined anticancer agents

On day 0, cells growing in the exponential phase were harvested with 0.05% trypsin and 0.02% EDTA and resuspended to a final concentration of 5.0×10^3 cells/ml in fresh medium containing 10% FBS and antibiotics. Cell suspensions (100 µl) were dispensed into the individual wells of a 96-well tissue culture plate (Falcon, Oxnard, Calif.). Each plate had one eight-well control column containing medium alone and one eight-well control column containing cells without drug. Eight plates were prepared for each drug combination. The cells were preincubated overnight to allow attachment.

Simultaneous exposure to pemetrexed and paclitaxel

After the overnight incubation for cell attachment, solutions of pemetrexed and paclitaxel (50 µl) at different concentrations were added to the individual wells. The plates were also incubated under the same conditions for 24 h. The cells were then washed twice with culture medium containing 1% FBS, and then fresh medium containing 10% FBS (200 µl) and antibiotics was added. The cells were incubated again for 4 days.

Sequential exposure to pemetrexed followed by paclitaxel or the reverse sequence

After overnight incubation, medium containing 10% FBS (50 µl) and solutions (50 µl) of pemetrexed (or paclitaxel) at different concentrations was added to individual wells. The plates were then incubated under the same conditions for 24 h. The cells were washed twice with culture medium containing 1% FBS; then fresh medium containing 10% FBS (150 µl) and antibiotics was added, followed by the addition of solutions (50 µl) of paclitaxel (or pemetrexed) at different concentrations. The plates were incubated again under the same conditions for 24 h. The cells were then washed twice with culture medium, and fresh medium containing 10% FBS (200 µl) and antibiotics was added. The cells were then incubated again for 3 days.

MTT assay

Viable cell growth was determined by the 3-(4,5-dimethylthiazol-2-yl)-2,5-diphenyltetrazolium bromide (MTT) assay as described previously [12]. For all four cell lines examined, we were able to establish a linear relationship between the MTT assay value and the cell number within the range shown.

Isobologram

The dose-response interactions between pemetrexed and paclitaxel for the MCF7, PA1 and WiDr cells were evaluated at the IC_{80} level by the isobologram method (Fig. 1) [32]. The IC_{80} was defined as the concentration of drug that produced 80% cell growth inhibition, i.e., an 80% reduction of absorbance. Since the A549 cells were resistant to pemetrexed and the IC_{80} level was not obtained, the interactions between pemetrexed and paclitaxel were evaluated at the IC_{50} level. We used the isobologram method of Steel and Peckham because this method can cope with any agents with unclear cytotoxic mechanisms and a variety of dose-response curves of anticancer agents [32]. The concept of the isobologram has been described in detail previously [11, 16].

Three isoeffect curves, mode I and mode II, were constructed, based upon the dose-response curves of pemetrexed and paclitaxel (Fig. 1). Mode I and mode II were generated by the assumption regarding overlap and non-overlap damage in combinations, respectively. Thus, when the data points of the drug combination fell within the area surrounded by mode I and/or mode II lines (i.e., within the envelope of additivity), the combination was described as additive. We used this envelope not only to evaluate the simultaneous exposure combinations of pemetrexed and paclitaxel, but also to evaluate the sequential exposure combinations, since the second agent under our experimental conditions could modulate the cytotoxicity of the first agent.

A combination that gives data points to the left of the envelope of additivity (i.e., the combined effect is caused by lower doses of the two agents than is predicted) can confidently be described as supraadditive (synergistic). A combination that gives data points to the right of the envelope of additivity, but within the square or on the line of the square can be described as subadditive (i.e., the combination is superior or equal to a single agent but is less than additive). A combination that gives data points outside the square can be described as protective (i.e., the combination is inferior in cytotoxic action to a single agent). A combination with both subadditive and/or protective interactions can confidently be described as antagonistic. The Steel and Peckham isobologram is generally more strict regarding synergism and antagonism than other methods.

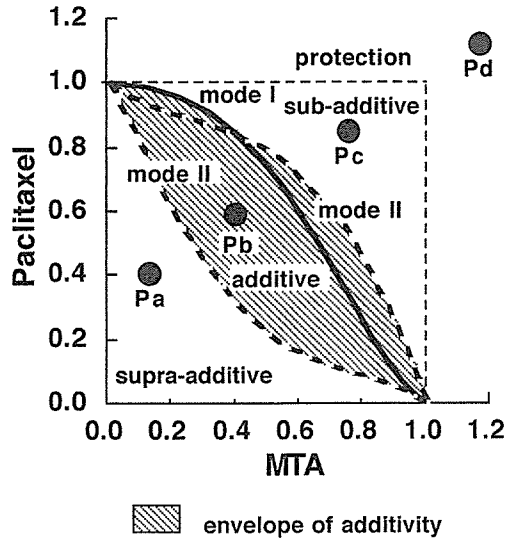

Fig. 1 Schematic representation of an isobologram (Steel and Peckham) [32]. The envelope of additivity, surrounded by mode I (*solid line*) and mode II (*dotted lines*) isobologram lines, was constructed from the dose-response curves of MTA and paclitaxel. The concentrations which produced 80% cell growth inhibition are shown as 1.0 on the ordinate and the abscissa of all isobolograms for MCF7, PA1, and WiDr cells, while the concentrations which produced 50% cell growth inhibition are shown as 1.0 on the ordinate and the abscissa of all isobolograms for A549 cells. Combined data points Pa, Pb, Pc, and Pd show supraadditive, additive, subadditive, and protective effects, respectively

Data analysis

The findings were analyzed as described previously [14]. When the observed data points of the combinations mainly fell in the area of supraadditivity or in the areas of subadditivity and protection, i.e., the mean value of the observed data was smaller than that of the predicted minimum values or larger than that of the predicted maximum values, the combinations were considered to have a synergistic or antagonistic effect, respectively. To determine whether the condition of synergism (or antagonism) truly existed, a statistical analysis was performed. The Wilcoxon signed-ranks test was used for comparing the observed data with the predicted minimum (or maximum) values for additive effects, which were closest to the observed data (i.e., the data on the boundary (mode I or mode II lines) between the additive area and supraadditive area (or subadditive and protective areas). Probability (P) values <0.05 were considered significant. Combinations with $P \geq 0.05$ were regarded as indicating additive to synergistic (or additive to antagonistic) effects. All statistical analyses were performed using the Stat View 4.01 software program (Abacus Concepts, Berkeley, Calif.).

Results

The IC_{80} values of pemetrexed for a 24-h exposure against MCF7, PA1, and WiDr cells were 3.3 ± 0.4, 0.15 ± 0.02, and 0.45 ± 0.04 μM, respectively, while those of paclitaxel against MCF7, PA1, and WiDr cells were 5.9 ± 0.4, 2.5 ± 0.06, and 5.8 ± 0.06 nM, respectively. The IC_{50} values of pemetrexed and paclitaxel for a 24-h exposure against A549 cells were 2.5 ± 0.3 μM and 3.4 ± 0.3 nM, respectively.

Figure 2 shows the dose-response curves obtained from simultaneous exposure and sequential exposure to pemetrexed and paclitaxel for the MCF7 cells. The

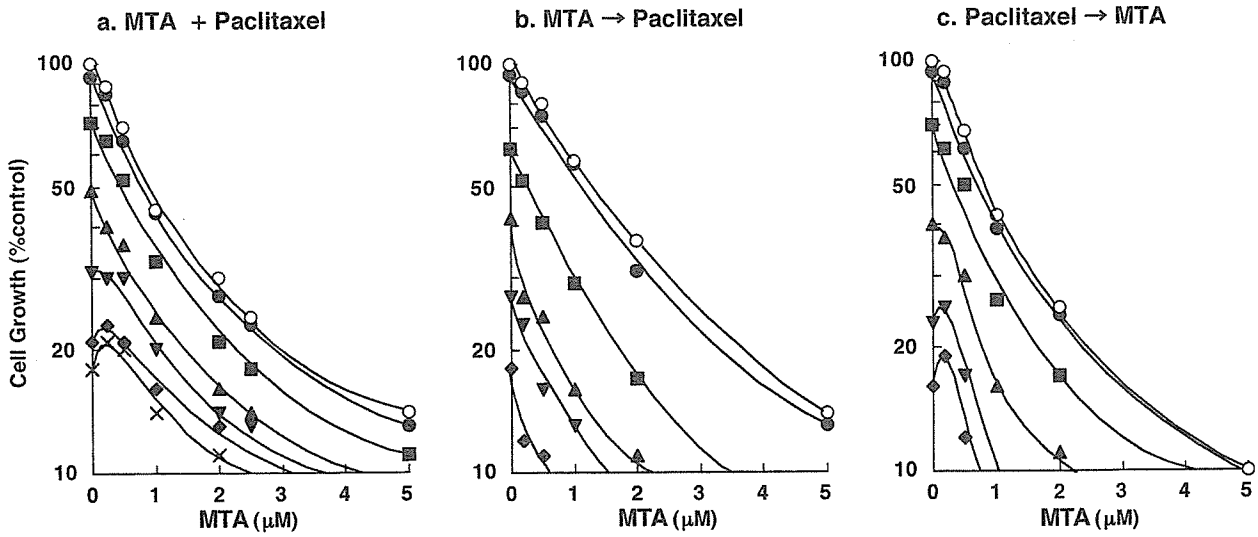

Fig. 2 Schedule dependence of the interaction between MTA and paclitaxel in MCF7 cells. Cells were exposed to (**a**) these two drugs simultaneously for 24 h, (**b**) MTA first for 24 h followed by paclitaxel for 24 h, or (**c**) the reverse sequence. The cell number after 5 days was measured using the MTT assay and was plotted as a percentage of the control (cells not exposed to drugs). The concentrations of MTA are shown on the abscissa. The concentrations of paclitaxel were 0 (*open circles*), 1 (*filled circles*), 2 (*filled squares*), 3 (*filled uptriangles*), 4 (*filled downtriangles*), 6 (*filled diamonds*), and 8 (*crosses*) n*M*, respectively. Data are the mean values for three independent experiments; SE was < 20%

dose-response curves were plotted on a semilog scale as a percentage of the control, the cell number of which was obtained from the samples not exposed to the drugs administered simultaneously. The pemetrexed concentrations are shown on the abscissa. Dose-response curves in which paclitaxel concentrations are shown on the abscissa could be made based on the same data (figure not shown).

Based upon the dose-response curves of pemetrexed alone and paclitaxel alone, three isoeffect curves (mode I and mode II lines) were constructed. Isobolograms at the IC_{80} and IC_{50} levels were generated based upon these dose-response curves for the combinations.

Simultaneous exposure to pemetrexed and paclitaxel for 24 h

Figure 3 shows the isobolograms of the A549, MCF7, PA1, and WiDr cells exposed to both agents simultaneously. For the A549 and PA1 cells, all or most combined data points fell in the areas of subadditivity and protection (Fig. 3a,c). The mean values of the data were larger than those of the predicted maximum data (Table 1). The differences were significant ($P < 0.05$ and $P < 0.05$), indicating antagonistic effects. For the MCF7 cells, the combined data points fell within the envelope of additivity and in the areas of subadditivity and protection (Fig. 3b; Table 1). The mean value of the data was larger than that of the predicted maximum data. The difference was not significant ($P \geq 0.05$), indicating additive/antagonistic effects. For the WiDr cells, the combined data points fell mainly within the envelope of additivity (Fig. 3d). The mean value of the data was larger than that of the predicted minimum data and smaller than that of the predicted maximum data (Table 1), indicating additive effects. A quite similar tendency was observed in the IC_{50} isobologram of the MCF7, PA1, and WiDr cells (not shown).

Sequential exposure to pemetrexed for 24 h followed by paclitaxel for 24 h

Figure 4 shows the isobolograms of the four cell lines exposed first to pemetrexed and then to paclitaxel. For the A549 and MCF7 cells, the combined data points fell in the area of supraadditivity and within the envelope of additivity (Fig. 4a,b). The mean values of the data were smaller than those of the predicted minimum data (Table 1). The differences were significant ($P < 0.05$ and $P < 0.05$), indicating synergistic effects. For the PA1 cells, the combined data points fell within the envelope of additivity (Fig. 4c), indicating additive effects (Table 1). For the WiDr cells, the combined data points fell within the envelope of additivity and in the area of supraadditivity (Fig. 4d). The mean value of the data was smaller than that of the predicted maximum data and larger than that of the predicted minimum data (Table 1), indicating additive effects. A quite similar tendency was observed in the IC_{50} isobologram of the MCF7, PA1, and WiDr cells (not shown).

Sequential exposure to paclitaxel for 24 h followed by pemetrexed for 24 h

Figure 5 shows the isobolograms of cells exposed first to paclitaxel and then to pemetrexed. For all four cell lines, all or most of the data points fell within the envelope of additivity, indicating additive effects (Table 1). A quite

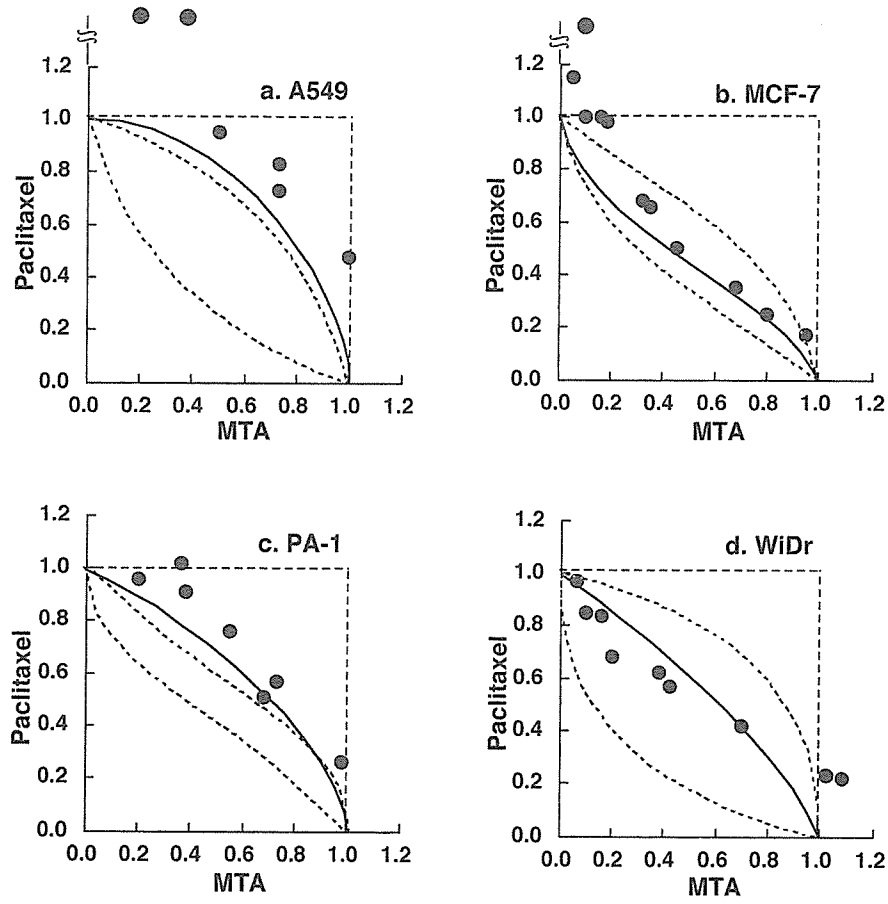

Fig. 3 Isobolograms of simultaneous exposure to MTA and paclitaxel for 24 h in (**a**) A549, (**b**) MCF7, (**c**) PA1, and (**d**) WiDr cells. For the A549, and PA1 cells, all or most combined data points fell in the areas of subadditivity and protection. For the MCF7 cells, combined data points fell within the envelope of additivity and in the areas of subadditivity and protection. For the WiDr cells, combined data points fell mainly within the envelope of additivity. Data are the mean values for at least three independent experiments; SE was <30%

similar tendency was observed in the IC_{50} isobologram of the MCF7, PA1, and WiDr cells.

Discussion

We studied the cytotoxic activity of various schedules of pemetrexed in combination with paclitaxel in culture to investigate the optimal schedule of this combination. The analysis of the effects of drug–drug interaction was carried out using the isobologram method of Steel and Peckham [32]. Among the solid tumor cell lines studied, PA1 was most sensitive to pemetrexed, while A549 was most resistant to pemetrexed. The pemetrexed concentrations required for IC_{80} and/or IC_{50} were well within the range that can be attained in human plasma using standard dosing regimens [23].

We demonstrated that cytotoxic interactions between pemetrexed and paclitaxel were schedule-dependent and cell line-dependent. Simultaneous exposure to pemetrexed and paclitaxel showed antagonistic effects in A549 and PA1 cells, additive/antagonistic effects in MCF7

Table 1 Mean values of observed data, predicted minimum, and predicted maximum values of MTA in combination with paclitaxel at IC_{80} for MCF7, PA1 and WiDr cells and at IC_{50} for A549 cells

Schedule	Cell line	*n*	Observed data	Predicted data for an additive effect		Effect
				Minimum	Maximum	
MTA + paclitaxel	A549	6	>0.92	0.22	0.69	Antagonism ($P<0.05$)
	MCF7	11	0.61	0.42	0.52	Additive/antagonism
	PA1	7	0.71	0.33	0.60	Antagonism ($P<0.05$)
	WiDr	9	0.61	0.29	0.78	Additive
MTA → paclitaxel	A549	8	0.31	0.36	0.80	Synergism ($P<0.05$)
	MCF7	8	0.45	0.60	0.66	Synergism ($P<0.05$)
	PA1	7	0.41	0.32	0.70	Additive
	WiDr	10	0.34	0.33	0.83	Additive
Paclitaxel → MTA	A549	6	0.78	0.31	0.82	Additive
	MCF7	8	0.58	0.44	0.66	Additive
	PA1	6	0.55	0.44	0.67	Additive
	WiDr	9	0.64	0.25	0.93	Additive

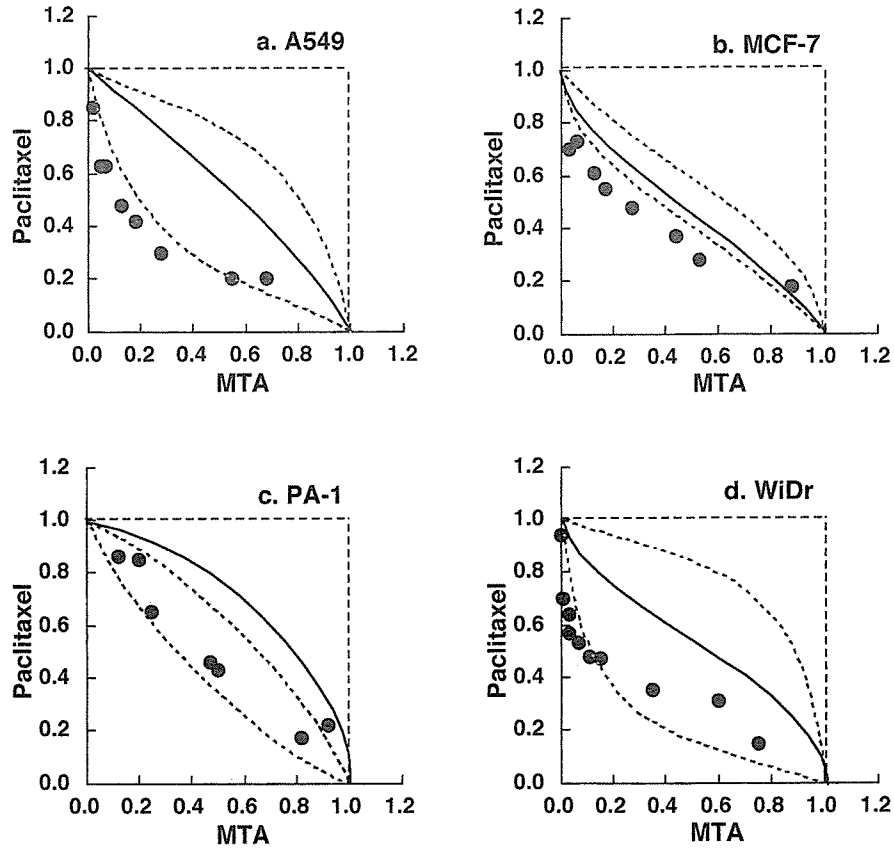

Fig. 4 Isobolograms of sequential exposure to MTA (24 h) followed by paclitaxel (24 h) in (**a**) A549, (**b**) MCF7, (**c**) PA1, and (**d**) WiDr cells. For the A549 and MCF7 cells, most data points of the combinations fell in the area of supraadditivity. For the PA1 cells, all the data points fell within the envelope of additivity. For the WiDr cells, the data points fell within the envelope of additivity and in the area of supraadditivity. Data are the mean values for at least three independent experiments; SE was <20%

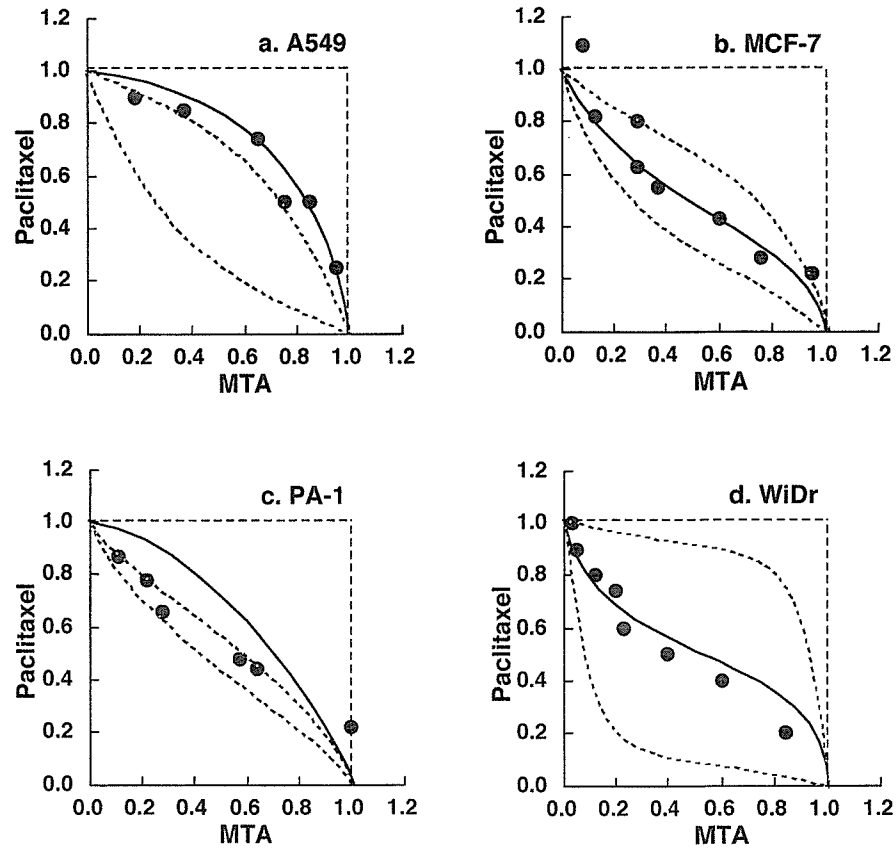

Fig. 5 Isobolograms of sequential exposure to paclitaxel (24 h) followed by MTA (24 h) in (**a**) A549, (**b**) MCF7, (**c**) PA1, and (**d**) WiDr cells. For all four cells, all or most data points of the combinations fell within the envelope of additivity. Data are the mean values for at least three independent experiments; SE was <25%

cells and additive effects in WiDr cells. Sequential exposure to pemetrexed for 24 h followed by paclitaxel showed synergistic effects in A549 and MCF7 cells and additive effects in PA1 and WiDr cells. However, the combined data points in PA1 and WiDr cells were close to the borderlines between supraadditive and additive areas (Fig. 4), and the observed data were close to the predicted minimum values for an additive effect (Table 1). The combined data points in WiDr cells fell both in the area of supraadditivity and within the envelope of additivity (Fig. 4). Since the isobologram of Steel and Peckham is more strict for synergism and antagonism than other methods for evaluating the effects of drug combinations, simultaneous exposure to pemetrexed and paclitaxel and sequential exposure to pemetrexed followed by paclitaxel would be defined as having antagonistic and synergistic effects, respectively, using other methods.

On the other hand, sequential exposure to paclitaxel followed by pemetrexed showed additive effects in all four cell lines tested. The results of flow cytometric analysis of PA1 cells were consistent with these findings. Enhanced apoptosis was observed only in the pemetrexed–paclitaxel sequence (data not shown).

Our findings suggest that the simultaneous administration of pemetrexed and paclitaxel on the same day is convenient for clinical use but is suboptimal. The sequential administration of pemetrexed followed by paclitaxel may be the optimal schedule for these combinations. For example, administrations of pemetrexed on day 1 and paclitaxel on day 2 would be worthy of clinical investigation. Several in vitro and in vivo studies of combinations of pemetrexed with paclitaxel have been reported [28, 34, 35]. Schultz et al. observed synergistic effects when pemetrexed exposure preceded paclitaxel exposure by 24 h, while the reverse order produced only additive effects in three human cancer cells in vitro [28]. Although the detailed experimental systems are not described in the abstract, our data support their findings.

Teicher et al. studied the combination of pemetrexed and paclitaxel in vivo against EMT-6 murine mammary carcinoma using a tumor cell survival assay [34]. They observed that pemetrexed administered four times over 48 h with paclitaxel administered with the third dose of pemetrexed produced an additive or more than additive tumor response. They further studied the combination of pemetrexed and paclitaxel in human tumor xenografts [35]. Administration of pemetrexed (days 7–11, days 14–18) along with paclitaxel (days 8, 10, 12, and 15) produced greater-than-additive effects on human lung cancer H460 tumor growth delay, while that of pemetrexed (days 7–11) along with paclitaxel (days 7, 9, 11, and 13) produced additive effects on human breast cancer MX-1 tumor growth delay. Since the schedules of administration of pemetrexed with paclitaxel were quite different from ours, comparison seems difficult.

The mechanisms underlying the schedule-dependent synergism and antagonism of the combination of pemetrexed and paclitaxel are unclear. Cell cycle analysis showed that initially exposing cells to pemetrexed leads to synchronization in the S phase (data not shown). Cells in the S phase are sensitive to paclitaxel, in addition to cells in G_2/M phase [17]. This may explain the synergistic effects of sequential exposure to pemetrexed followed by paclitaxel. Simultaneous exposure to pemetrexed and paclitaxel produced antagonistic effects. Pemetrexed has a cytotoxic effect by blocking cells in the S phase [38], while paclitaxel has cytotoxic effects by blocking cells in the G_2/M phase [17, 27]. Thus, one agent might reduce the cytotoxicity of the other agent by preventing cells from entering the specific phase in which the cells are most cytotoxic to the other agent. Interestingly, we have observed similar cytotoxic interactions between methotrexate and paclitaxel [15]. Simultaneous exposure to methotrexate and paclitaxel produces antagonistic effects, while the methotrexate/paclitaxel sequence produces synergistic effects and the reverse sequence produces additive effects. These experimental data suggest that antifolates, which inhibit dihydrofolate reductase, may enhance the cytotoxic action of paclitaxel in sequential administration.

It should be noted that in vitro studies cannot evaluate toxic and pharmacokinetic interactions. Thus, in vivo studies are required to confirm whether the pemetrexed–paclitaxel sequence is optimal or not. In clinical oncology, drug interaction may result in synergism, not only in terms of efficacy but also in terms of toxic side effects. If the toxicities of the drug combinations were compared between the schedules of synergistic and antagonistic interactions at the same doses, the schedules with antagonistic interactions may produce less toxicity than the schedules with synergistic interactions. Our data showed that the drug doses required for IC_{80} or IC_{50} levels with sequential exposure to pemetrexed followed by paclitaxel are less than 70% of the drug doses required for IC_{80} or IC_{50} with simultaneous exposure to the two agents (Figs. 3 and 4). This suggests that the optimal doses for sequential administration of pemetrexed followed by paclitaxel may be lower than those for the simultaneous administration of the two agents. This is important and must be kept in mind for translating in vitro data to clinical applications, since the schedule showing antagonistic effects of the combination may be selected because of less toxicity during the first stage of clinical study.

In conclusion, our findings suggest that the cytotoxic effects of the combination of pemetrexed and paclitaxel are schedule-dependent. The optimal schedule of pemetrexed in combination with paclitaxel is the sequential administration of pemetrexed followed by paclitaxel. Although there are a number of difficulties in the translation of results from in vitro to clinical therapy, this schedule should be assessed in clinical trials for the treatment of solid tumors.

Acknowledgments This work was supported in part by a Grant-in-Aid for Cancer Research (11-8) from the Ministry of Health and Welfare and by a Grant-in-Aid for Research on the Second-Term

Comprehensive 10-Year Strategy for Cancer Control from the Ministry of Health and Welfare of Japan.

References

1. Arbuck SG (1995) Paclitaxel: current developmental approaches of the National Cancer Institute. Semin Oncol 22:55–56
2. Britten CD, Izbicka E, Hilsenbeck S, Lawrence R, Davidson K, Cerna C, Gomez L, Rowinsky EK, Weitman S, Van Hoff DD (1999) Activity of the multitargeted antifolate MTA in the human tumor cloning assay. Cancer Chemother Pharmacol 44:105–110
3. Calvert AH, Walling JM (1998) Clinical studies with MTA. Br J Cancer 78 [Suppl 3]:35–40
4. Celio L, Buzzoni R, Longarini R, Marchiano A, Bajetta E (2002) Pemetrexed in gastric cancer: clinical experience and future perspectives. Semin Oncol 29 [Suppl 18]:63–68
5. Chen VJ, Bewley JR, Smith PG, Andis SL, Schultz RM, Iversen PW, Tonkinson JL, Shih C (2000) An assessment of the antithymine and antipurine characteristics of MTA (LY231514) in CCRF-CEM cells. Adv Enzyme Regul 40:143–154
6. Donehower RC, Rowinsky EK (1993) An overview of experience with taxol (paclitaxel) in the USA. Cancer Treat Rev 19 [Suppl C]:63–78
7. Habeck LL, Mendelsohn LG, Shih C, Taylor EC, Colman PD, Gossett LS, Leitner TA, Schultz RM, Andis SL, Moran RG (1995) Substrate specificity of mammalian folypolyglutamate synthetase for 5,10-dideazatetrahydrofolate analogs. Mol Pharmacol 48:326–333
8. Haller DG (2002) Future directions in the treatment of pancreatic cancer. Semin Oncol 29 [Suppl 20]:31–39
9. Hanauske AR, Chen V, Paoletti P, Niyikiza C (2001) Pemetrexed disodium: a novel antifolate clinically active against multiple solid tumors. Oncologist 6:363–373
10. Hochster H (2002) The role of pemetrexed in the treatment of colorectal cancer. Semin Oncol 29 [6 Suppl 18]:54–56
11. Kano Y, Ohnuma T, Okano T, Holland JF (1988) Effects of vincristine in combination with methotrexate and other antitumor agents in human acute lymphoblastic leukemia cells in culture. Cancer Res 48:351–356
12. Kano Y, Sakamoto S, Kasahara T, Akutsu M, Inoue Y, Miura Y (1991) In vitro effects of amsacrine in combination with other anticancer agents. Leuk Res 15:1059–1064
13. Kano Y, Akutsu M, Tsunoda S, Ando J, Matsui J, Suzuki K, Ikeda T, Inoue Y, Adachi K (1996) Schedule-dependent interaction between paclitaxel and 5-fluorouracil in human carcinoma cell lines in vitro. Br J Cancer 74:704–710
14. Kano Y, Akutsu M, Tsunoda S, Suzuki K, Adachi K (1998) In vitro schedule-dependent interaction between paclitaxel and SN-38 (the active metabolite of irinotecan) in human carcinoma cell lines. Cancer Chemother Pharmacol 42:91–98
15. Kano Y, Akutsu M, Tsunoda S, Furuta M, Yazawa Y, Ando J (1998) Schedule-dependent synergism and antagonism between paclitaxel and methotrexate in human carcinoma cell lines. Oncol Res 10:347–354
16. Kano Y, Akutsu M, Tsunoda S, Mano H, Sato Y, Honma Y, Furukawa Y (2001) In vitro cytotoxic effects of a tyrosine kinase inhibitor STI571 in combination with commonly used antileukemic agents. Blood 97:1999–2007
17. Lieu CH, Chang YN, Lai YK (1997) Dual cytotoxic mechanisms of submicromolar taxol on human leukemia HL-60 cells. Biochem Pharmacol 53:1587–1596
18. McDonald AC, Vasey PA, Adams L, Walling J, Woodworth JR, Abrahams T, McCarthy S, Bailey NP, Siddiqui N, Lind MJ, Calvert AH, Twelves CJ, Cassidy J, Kaye SB (1998) A phase I and pharmacokinetic study of LY231514, the multitargeted antifolate. Clin Cancer Res 4:605–610
19. O'Shaughnessy JA, Gennari A, Conte P (2002) Pemetrexed: a promising new treatment for breast cancer. Semin Oncol 29 [2 Suppl 5]:36–41
20. Paz-Ares L, Ciruelos E, Garcia-Carbonero R, Castellano D, Lopez-Martin A, Cortes-Funes H (2002) Pemetrexed in bladder, head and neck, and cervical cancers. Semin Oncol 29 [Suppl 18]:69–75
21. Paz-Ares L, Bezares S, Tabernero JM, Castellanos D, Cortes-Funes H (2003) Review of a promising new agent—pemetrexed disodium. Cancer [Suppl] 97:2056–2063
22. Raymond E, Louvet C, Tournigand C, Coudray AM, Faivre S, De Gramont A, Gespach C (2002) Pemetrexed disodium combined with oxaliplatin, SN38, or 5-fluorouracil, based on the quantitation of drug interactions in human HT29 colon cancer cells. Int J Oncol 21:361–367
23. Rinaldi DA (1999) Overview of phase I trials of multitargeted antifolate (MTA, LY231514). Semin Oncol 26 [Suppl 6]:82–88
24. Rinaldi DA, Burris HA, Dorr FA, Woodworth JR, Kuhn JG, Eckardt JR, Rodriguez G, Corso SW, Fields SM, Langley C, Clark G, Faries D, Lu P, Van Hoff DD (1995) Initial phase I evaluation of the novel thymidylate synthase inhibitor, LY231514, using the modified continual reassessment method for dose escalation. J Clin Oncol 13:2842–2850
25. Rinaldi DA, Kuhn JG, Burris HA, Dorr FA, Rodriguez G, Eckhardt SG, Jones S, Woodworth JR, Baker S (1999) A phase I evaluation of multitargeted antifolate (MTA, LY231514), administered every 21 days, utilizing the modified continual reassessment method for dose escalation. Cancer Chemother Pharmacol 44:372–380
26. Scagliotti GV, Shin DM, Kindler HL, Vasconcelles MJ, Keppler U, Manegold C, Burris H, Gatzemeier U, Blatter J, Symanowski JT, Rusthoven JJ (2003) Phase II study of pemetrexed with and without folic acid and vitamin B_{12} as front-line therapy in malignant pleural mesothelioma. J Clin Oncol 21:1556–1561
27. Schiff PB, Fant J, Horwitz SB (1979) Promotion of microtubule assembly in vitro by taxol. Nature 277:665–667
28. Schultz RM, Dempsey JA, Kraus LA, Schmid SM, Calvete JA, Laws AL (1999) In vitro sequence dependence for the multitargeted antifolate (MTA, LY231514) combined with other anticancer agents. Eur J Cancer 35 [Suppl 4]:S194
29. Shih C, Thornton DE (1998) Preclinical pharmacology studies and the clinical development of a novel multitargeted antifolate, MTA (LY231514). In: Jackman AL (ed) Anticancer drug development guide: antifolate drugs in cancer therapy. Humana, Totowa, p 183
30. Shih C, Chen VJ, Gossett LS, Gates SB, MacKellar WC, Habeck LL, Shackelford KA, Mendelsohn LG, Soose DJ, Patel VF, Andis SL, Bewley JR, Rayl EA, Moroson BA, Beardsley GP, Kohler W, Ratnam M, Schultz RM (1997) LY231514, a pyrrolo[2,3-d]pyrimidine-based antifolate that inhibits multiple folate-requiring enzymes. Cancer Res 57:1116–1123
31. Shih C, Habeck LL, Mendelsohn LG, Chen VJ, Schultz RM (1998) Multiple folate enzyme inhibition: mechanism of a novel pyrrolopyrimidine-based antifolate LY231514 (MTA). Adv Enzyme Regul 38:135–152
32. Steel GG, Peckham MJ (1979) Exploitable mechanisms in combined radiotherapy–chemotherapy: the concept of additivity. Int J Radiat Oncol Biol Phys 5:85–91
33. Taylor EC, Kuhnt D, Shih C, Rinzel SM, Grindey GB, Barredo J, Jannatipour M, Moran RG (1992) A dideazatetrahydrofolate analogue lacking a chiral center at C-6, *N*-[4-[2-(2-amino-3,4-dihydro-4-oxo-7H-pyrrolo[2,3-d]pyrimidin-5-yl)ethyl]benzoyl]-L-glutamic acid, is an inhibitor of thymidylate synthase. J Med Chem 35:4450–4454
34. Teicher BA, Alvarez E, Liu P, Lu K, Menon K, Dempsey J, Schultz RM (1999) MTA (LY231514) in combination treatment regimens using human tumor xenografts and the EMT-6 murine mammary carcinoma. Semin Oncol 28:55–62
35. Teicher BA, Chen V, Shih C, Menon K, Forler PA, Phares VG, Amsrud T (2000) Treatment regimens including the multitargeted antifolate LY231514 in human tumor xenografts. Clin Cancer Res 6:1016–1023

36. Tesei A, Ricotti L, De Paola F, Amadori D, Frassineti GL, Zoli W (2002) In vitro schedule-dependent interactions between the multitargeted antifolate LY231514 and gemcitabine in human colon adenocarcinoma cell lines. Clin Cancer Res 8:233–239
37. Tomek S, Emri S, Krejcy K, Manegold C (2003) Chemotherapy for malignant pleural mesothelioma: past results and recent developments. Br J Cancer 88:167–174
38. Tonkinson JL, Marder P, Andis SL, Schultz RM, Gossett LS, Shih C, Mendelsohn LG (1997) Cell cycle effects of antifolate antimetabolites: implications for cytotoxicity and cytostasis. Cancer Chemother Pharmacol 39:521–531
39. Vogelzang NJ, Rusthoven JJ, Symanowski J, Denham C, Kaukel E, Ruffie P, Gatzemeier U, Boyer M, Emri S, Manegold C, Niyikiza C, Paoletti P (2003) Phase III study of pemetrexed in combination with cisplatin versus cisplatin alone in patients with malignant pleural mesothelioma. J Clin Oncol 21:2636–2644

[Cancer Biology & Therapy 3:1, 96-101, January 2004]; ©2004 Landes Bioscience

Research Paper

The Tyr-Kinase Inhibitor AG879, That Blocks the ETK-PAK1 Interaction, Suppresses the RAS-Induced PAK1 Activation and Malignant Transformation

Hong He[1]
Yumiko Hirokawa[1]
Aviv Gazit[2]
Yoshihiro Yamashita[3]
Hiroyuki Mano[3]
Yuko Kawakami[4]
Kawakami[4]
Ching-Yi Hsieh[5]
Hsing-Jien Kung[5]
Guillaume Lessene[6]
Jonathan Baell[6]
Alexander Levitzki[2]
Hiroshi Maruta[1,*]

[1]Ludwig Institute for Cancer Research; Royal Melbourne Hospital; Parkville/Melbourne, Australia

[2]Department of Biological Chemistry; The Alexander Silverman Institute of Life Sciences; Hebrew University of Jerusalem; Jerusalem, Israel,

[3]Division of Functional Genomics; Jichi Medical School; Tochigi, Japan

[4]La Jolla Institute for Allergy and Immunology; San Diego, California USA

[5]Cancer Center; University of California at Davis; Sacramento, California USA

[6]Walter and Eliza Hall Institute for Medical Research; Parkville/Melbourne, Australia

*Correspondence to: Hiroshi Maruta; Ludwig Institute for Cancer Research; P.O. Box 2008 Royal Melbourne Hospital; Parkville/Melbourne, Australia 3050; Tel.: 613.9341.3155; Fax: 613.9341.3104; Email: Hiroshi.maruta@ludwig.edu.au

Received 09/16/03; Accepted 10/29/03

Previously published online as a *Cancer Biology & Therapy* E-publication: http://www.landesbioscience.com/journals/cbt/abstract.php?id=643

KEY WORDS

AG879, ETK, RAS, PAK, transformation

ACKNOWLEDGEMENTS

We thank Mrs. Thao Nheu and Dr. Hong-jian Zhu for their generous gift of a doxycycline-inducible RAS transformant of NIH/3T3 cells; Dr. Yun Qiu for her generous gift of the ETK PH domain construct in a pGEX vector; Dr. Nathan Hall for his comparison of the 3D structure of the kinase domain between ETK, BTK and TEC by a molecular modelling; and Prof. Tony Burgess for his consistent support and advice throughout this work.

ABSTRACT

AG 879 has been widely used as a Tyr kinase inhibitor specific for ErbB2 and FLK-1, a VEGF receptor. The IC_{50} for both ErbB2 and FLK-1 is around 1 μM. AG 879, in combination of PP1 (an inhibitor specific for Src kinase family), suppresses almost completely the growth of RAS-induced sarcomas in nude mice. In this paper we demonstrate that AG 879 even at 10 nM blocks the specific interaction between the Tyr-kinase ETK and PAK1 (a CDC42/ Rac-dependent Ser/Thr kinase) in cell culture. This interaction is essential for both the RAS-induced PAK1 activation and transformation of NIH 3T3 fibroblasts. However, AG 879 at 10 nM does not inhibit either the purified ETK or PAK1 directly in vitro, suggesting that this drug blocks the ETK-PAK1 pathway by targeting a highly sensitive kinase upstream of ETK. Although the Tyr-kinases Src and FAK are known to activate ETK directly, Src is insensitive to AG 879, and FAK is inhibited by 100 nM AG 879, but not by 10 nM AG879. The structure-function relationship analysis of AG 879 derivatives has revealed that both thio and tert-butyl groups of AG 879, but not (thio) amide group, are essential for its biological function (blocking the ETK-PAK1 pathway), suggesting that through the (thio) amide group, AG 879 can be covalently linked to agarose beads to form a bioactive affinity ligand useful for identifying the primary target of this drug.

INTRODUCTION

PAK1, a member of CDC42/Rac-dependent Ser/Thr kinase family (PAKs), is activated by oncogenic RAS mutants such as v-Ha-RAS, and is essential for RAS-transformation of fibroblasts such as Rat-1 and NIH 3T3 cells.[1,2] Several distinct pathways appear to be essential for v-Ha-RAS-induced activation of PAK1 in these cells.[2] One of these pathways involves PI-3 kinase which produces phosphatidyl-inositol 3,4,5 trisphosphate (PIP3) that activates both CDC42 and Rac GTPases through a GDP-dissociation stimulator (GDS) called VAV. A second pathway involves PIX, an SH3 protein which binds a Pro-rich motif (residues 186-203, PAK18) located between the N-terminal GTPase-binding domain and C-terminal kinase domain of PAK1.[3] PIX binds another protein called CAT which is a substrate of Src family kinases.[4] A third pathway involves an SH2/SH3 adaptor protein called NCK.[5] The SH3 domain of NCK binds another Pro-rich motif of PAK1 located near the N-terminus, while the SH2 domain of NCK binds the Tyr-phosphorylated EGF receptor/ErbB1.[5] Thus, when ErbB1 is activated by EGF, PAK1 is translocated to the plasma membrane through NCK. The involvement of both Src family kinases and ErbB1 in the PAK1 activation is also supported by our finding that both PP1 (inhibitor of Src family kinases) and AG1478 (ErbB1-specific inhibitor) block the RAS-induced PAK1 activation and transformation in vitro and in vivo.[2,6] A fourth pathway involves ErbB2, a member of ErbB family Tyr kinases.[2] We have previously shown that AG 825 (ErbB2-specific inhibitor) blocks RAS-induced activation of PAK1 and malignant transformation with the IC_{50} around 0.35 μM.[2] A fifth pathway has been recently discovered in which RAS activates PAK1 through Tiam1, a Rac-specific GDS , in a PI-3 kinase-independent manner.[7] In this pathway, RAS directly binds Tiam1 which in turn activates Rac.[7]

Another possible pathway involves β1-integrin, FAK and ETK. β1-integrin activates the Tyr kinase FAK, which in turn phosphorylates and activates ETK,[8] a member of TEC/BTK family Tyr kinases.[9,10] ETK carries an N-terminal pleckstrin homology (PH) domain followed by a TEC homology domain.[9,10] Activated ETK binds PAK1 through the PH domain, phosphorylates and activates PAK1.[11] However, it still remains to be

clarified (1) whether RAS requires this integrin/FAK/ ETK pathway for its oncogenicity, and (2) how RAS activates this pathway.

To suppress the growth of RAS-induced sarcomas in vivo (in nude mice), we previously used AG 879, a Tyr-kinase inhibitor specific for ErbB2 and VEGF receptor FLK-1.[2,12,13] In this paper we demonstrate that AG879 inhibits selectively the activation of ETK (IC_{50} around 5 nM), blocking RAS-induced ETK-mediated activation (Tyr phosphorylation) of PAK1 to suppress RAS transformation.

MATERIALS AND METHODS

Cell Culture and Reagents. v-Ha-RAS-transformed NIH 3T3 fibroblasts (RAS cells) were grown in a standard medium, i.e., Dulbecco's modified Eagle's medium in the presence or absence of 10% fetal calf serum as described previously.[2,6] The Tyr kinase inhibitor AG879 and its derivatives (AG 306 and AG 1584) were synthesized as described previously.[12] The novel derivative GL-2002 was synthesized analogously, and full synthetic details will be published in due course. Two other AG 879 derivatives (AG 99 and AG 213) were purchased from Calbiochem (Croydon, Australia). The following antibodies were obtained from Santa Cruz Biotechnology (Santa Cruz,CA): anti-PAK1 antibody, anti-phospho-Tyr antibody (PY99) and goat-anti-ETK antibody. The rabbit anti-FAK antibody was a generous gift of Dr. David Schlaepfer (The Scripps Research Institute, La Jolla, CA). The mouse anti-ETK antibody was purchased from Becton Dickinson Biosciences (North Ryde, NSW, Australia). The rabbit anti-ETK antibody was prepared as described previously.[14]

Assay for the Effect of AG 879 on Cell Growth. The effect of AG879 on anchorage-independent growth of RAS cells was determined by seeding 10^3 cells per plate into 0.35% top agar containing different concentrations of AG879 (from 1 nM to 1 μM) and incubating for 3 weeks as described previously.[2,6,15] At the end of 3 weeks, the colonies formed in the agar were stained and counted. The effect of AG 879 on anchorage-dependent growth of RAS cells and normal NIH/3T3 fibroblasts was examined by seeding 10^3 cells per plate in the medium containing 1–100 nM AG 879, incubating for 5 days and counting as described previously.[2,6,15]

PAK and ETK Kinase Assays. For the PAK kinase assay, RAS cells were serum-starved overnight, and then treated with different concentrations of AG879 for 1 hour as described in the text. The cells were lysed in the lysis buffer (40 mM HEPES, pH 7.4, 1% Nonidet P-40, 1 mM EDTA, 100 mM NaCl, 25 mM NaF, 100 μM $NaVO_3$, 1 mM phenylmethylsulfonyl fluoride (PMSF), and 100 units/ml aprotinin). The lysates containing 1 mg of proteins (measured by Bradford assay) were immuno-precipitated with the anti-PAK1 antibody, and the immuno-precipitates were subjected to the PAK kinase assay as described previously.[1,2,6,16] The direct effect of AG 879 on PAK1 was determined in vitro, using GST-PAK1 fusion protein as described previously.[17] For ETK kinase assay, serum-starved RAS cells were lysed in a buffer containing 20 mM Tris-HCl (pH 7.5), 100 mM NaCl, 10% glycerol, 1% Nonidet P-40, 10 mM NaF, 100 μM $NaVO_3$, 1 mM PMSF, and 100 units/ml aprotinin. The cell lysates were immuno-precipitated with the rabbit anti-ETK antibody, and the ETK kinase assay was performed as described previously[8,11] using the endogenous PAK1 associated with ETK as a substrate in the presence or absence of different concentrations of AG879 or its derivatives such as AG 1584. Immuno-blotting was performed to determine the protein levels for PAK1 and ETK (see below).

Immuno-Precipitation and Immuno-Blotting. Serum-starved RAS cells were treated with different concentrations of AG879 as indicated in the text. The cells were lysed in two different lysis buffers mentioned above. The cell lysates containing 1.5–2.0 mg of protein (measured by Bradford assay) were incubated with protein A-Sepharose beads (Amersham Pharmacia Biotech) and anti-PAK1, anti-ETK or anti-FAK antibodies separately.[2,8,11,18] The proteins in immuno-precipitates were separated on 4–12% NuPage gel (Invitrogen) electrophoresis and transferred to a nitrocellulose membrane (Micron Separations, Inc.). The membranes were blocked with 10% (w/v) skim milk in phosphate-buffered saline containing 0.04% Tween20 (PBST), followed by an incubation for 1 hr at room temperature with different first antibodies as described in the text. After washing with PBST, the blots were incubated with horseradish peroxidase-conjugated anti-mouse or anti-rabbit (Bio-Rad) secondary antibodies. The bound antibodies were visualised using ECL reagents (Amersham Pharmacia Biotech). Some membranes were stripped and reblotted[19] with different antibodies as described in the text.

The ETK Baculo Viral Construct and its Affinity-Purification. The plasmid encoding the full-length ETK (residues 1-674)[14] was constructed in pBacPAK8 transfer vector (Clontech, Palo Alto, CA) and recombinant virus was made by Dr. Chi-Ying F. Huang (NHRI, Taiwan). Sf9 insect cells infected with the recombinant virus were harvested and disrupted with ice-cold lysis buffer containing 10 mM Tris pH, 7.5; 130 mM NaCl; 1% Triton X-100; 10 mM NaF; 10 mM Na phosphate; 10 mM Na pyro-phosphate and protease inhibitor cocktail (Pharmingen, San Diego, CA). From the clear supernatant of the cell lysate obtained by centrifuging at 40,000xg for 45 min, ETK was affinity-purified by the 6xHis purification kits (Cat. No. 21474K, Pharmingen, San Diego, CA) according to the supplier's instruction.

Autophosphorylation of Recombinant ETK Constructs In Vitro. GST fusion protein of human ETKC, a constitutively activated ETK mutant (residues 243–674) which lacks the N-terminal PH domain was affinity-purified from bacteria (E. coli). The GST-ETKC (0.6 μg) was incubated in the kinase buffer containing 10 μM ATP (with or without 5 μCi of [γ-^{32}P]-ATP) as described previously[8] in the presence or absence of AG879 (10 nM or 1–10 mM) at 37°C for 40 min. The auto-phosphorylation was then monitored by immuno-blotting the protein separated by the SDS-PAGE and transferred onto nitrocellulose with anti-phospho-Tyr antibody (or by radio-autography). Similarly 3 μg of full-length ETK purified from the insect cells was incubated in the buffer containing 30 mM PIPES, pH 7.0, 10 μM $MnCl^2$, 30 μM ATP, 5 μCi of [γ -^{32}P] ATP, 1 mM Na_3VO_4 for 20 min at 30°C, in the presence or absence of AG879 (10 nM–1 mM), and the auto-phosphorylation was measured by radio-autography of the proteins separated on SDS-PAGE.

Upregulation of ETK by RAS. The ETK protein levels were compared between normal NIH/3T3 cells and two distinct v-Ha-RAS transformed cell lines, excluding the possible clonal difference in the ETK levels: stable v-Ha-RAS cell line (RAS cells) and doxycycline-inducible v-Ha-RAS transformants prepared as described previously.[20,21] The lysates of both normal and RAS cells (20 μg protein of each) were subjected to SDS-PAGE and immuno-blotted by the anti-ETK antibody. In the case of doxycycline-inducible RAS transformants, cells were incubated for 2–3 days in the presence or absence of 2 μg/ml doxycycline, and each lysate (20 μg protein) was subjected to the SDS-PAGE/ immuno-blot with the anti-ETK.

RESULTS

AG879 (10 nM) Blocks the Activation of PAK1 and Suppresses RAS-Induced Malignant Transformation. AG879 was reported as an inhibitor specific for both ErbB2 and VEGF receptor FLK-1 (IC50 is around 1 mM)[12,13] and appears to be metabolically more stable than AG825 in vivo as it strongly suppresses the growth of RAS-sarcomas in nude mice.[2] However, the IC_{50} of AG879 for inhibiting PAK1 activation and RAS transformation in vitro still remained to be determined.

10 nM AG879 strongly blocks PAK1 kinase activity in RAS cells without affecting the PAK1 protein level (Fig. 1A). However, AG879 does not inhibit the kinase activity of the purified GST-PAK1 fusion protein directly even at 1 μM (Fig. 1B). These observations suggest that ErbB2 is not involved in the inactivation by AG879 of PAK1 in cells. Interestingly, AG879 also suppresses the anchorage-independent growth of RAS cells in soft agar (Fig. 1C). The IC_{50} of AG879 for the large colony formation is 1–10 nM. However, the inhibition of anchorage-independent growth by AG879 is not due to non-specific inhibition on cell growth, as at even 100

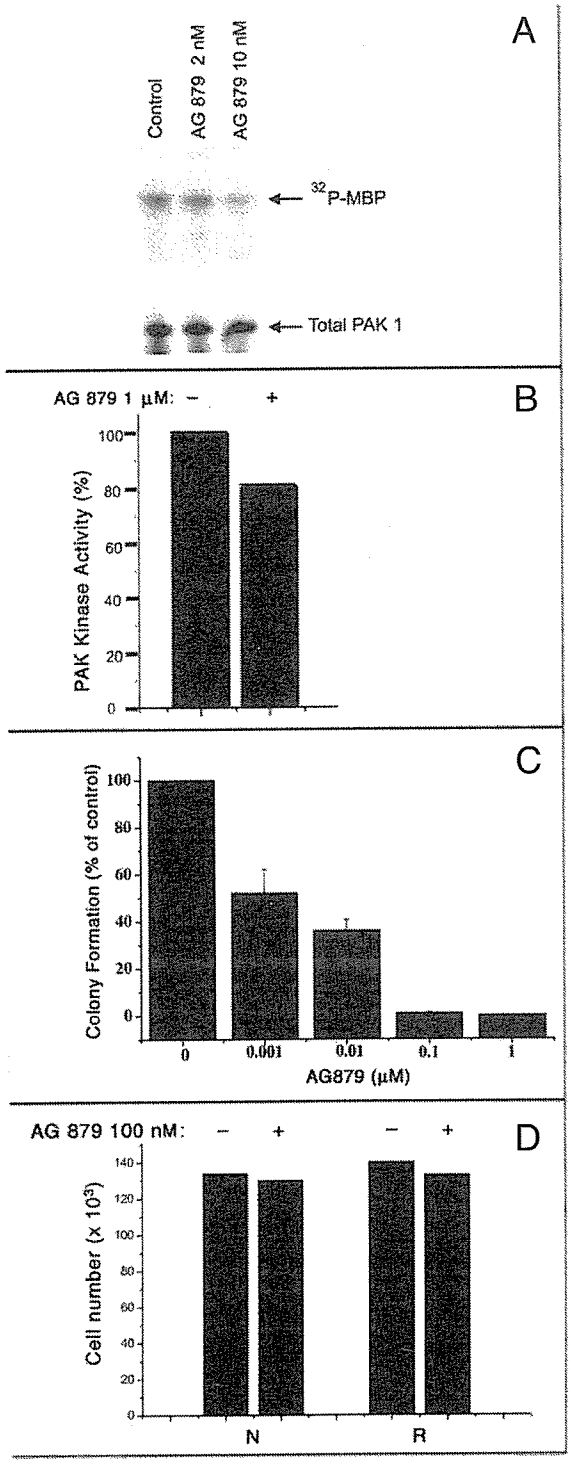

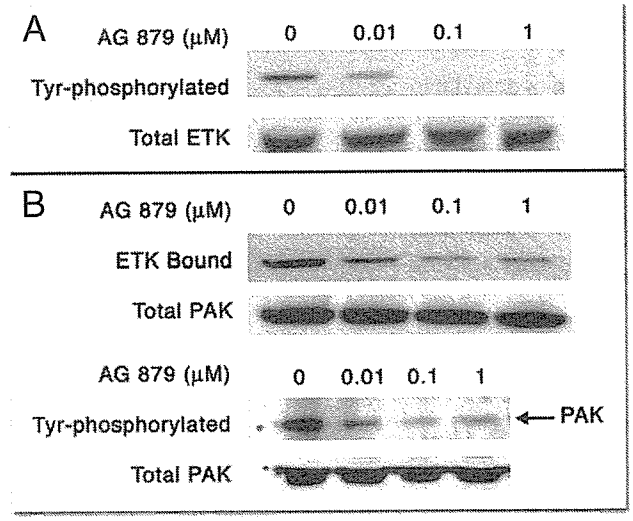

Figure 2. AG879 blocks the Tyr-phosphorylation of ETK and its association with PAK1. (A) Serum-starved RAS cells were first incubated with AG879 (0.01-1 μM) for 1hr. The cells lysates (CL) were then immuno-precipitated (IP) with the anti-ETK antibody as described under "Materials & Methods", followed by immuno-blot (IB) with anti-phospho-Tyr (PY) antibody. (B) Alternatively, the CL were IP with the anti-PAK1 (top panel) or anti-PY (bottom panel) antibodies, followed by IB with anti-ETK (top panel) or anti-PAK1 (bottom panel) antibodies. The total PAK1 protein level of the bottom panel was determined by IBing each CL directly. Similar results were obtained from two or three independent experiments.

nM AG879 does not affect the anchorage-dependent growth of either normal or RAS-transformed NIH 3T3 cells (Fig. 1D). These results suggest that the suppression by AG 879 of both RAS-induced malignant transformation and PAK1 activation is not due to blocking ErbB2, but another kinase(s) associated with PAK1.

AG879 Inhibits the Tyr-Phosphorylation of ETK and Its Association with PAK1. The Tyr-phosphorylation of PAK1 is required for its Ser/Thr kinase activity as the treatment of PAK1with a Tyr-phosphatase reduces its kinase activity.[22] Activated ETK associates with PAK1 through its PH domain and activates PAK1 by the Tyr phosphorylation.[11] To test whether the Tyr kinase activity of ETK is affected by AG879, serum-starved RAS cells were treated with AG879 (0.01–1 μM) in culture for 1hr. Cell lysates were then immuno-precipitated with the anti-ETK antibody, followed by immuno-blotting with the anti-phospho-Tyr or anti-ETK antibody. AG879 inhibits the Tyr-phosphorylation of ETK at 10 nM, but does not affect the ETK protein level (Fig. 2A). Furthermore, using the anti-PAK1 antibody, we found that AG879 significantly suppresses the ETK-PAK1 association (Fig.2B, top panel) and reduced the Tyr-phosphorylation of PAK1 in cells at 10 nM (Fig.2B, bottom panel). These results suggest that AG879 inhibits somehow the kinase activity of ETK, thus blocking its auto-phosphorylation, and association with PAK1, and the Tyr-phosphorylation of PAK1 by ETK.

AG879 Inactivates ETK In Vitro. To determine whether AG879 directly inhibits the kinase activity of ETK or not, RAS cells were lysed and

Figure 1. (A) AG879 inhibits the activation of PAK1 in cells. Serum-starved RAS cells were incubated with AG879 (0.01–10 μM) for 1hr. The cell lysates were subjected to PAK kinase assay as described under "Materials & Methods". 10 nM AG 879 clearly inhibited the PAK1 activity (phosphorylation of MBP) in cells (top panel). Similar levels of PAK1 protein were detected in all lanes as judged by immuno-blot (bottom panel). (B) PAK1 is not a direct target of AG 879. 1 μM AG 879 fails to inhibit significantly the kinase activity of GST-PAK1 in vitro. (C) AG879 inhibits anchorage-independent growth of RAS cells. RAS cells were planted in soft agar with or without AG879 (0.001—100 μM) as described under "Materials & Methods". The colony formation was measured in comparison with that of the control (non-treated) cells. Only large colonies consisting more than 100 cells per colony were counted. The presented values are the average of those obtained from two independent experiments. (D) AG 879 has no effect on the anchorage-dependent cell growth. The growth of either normal or RAS-transformed cells in liquid culture was monitored in the presence or absence of 100 nM AG 879 as described under "Materials & Methods".

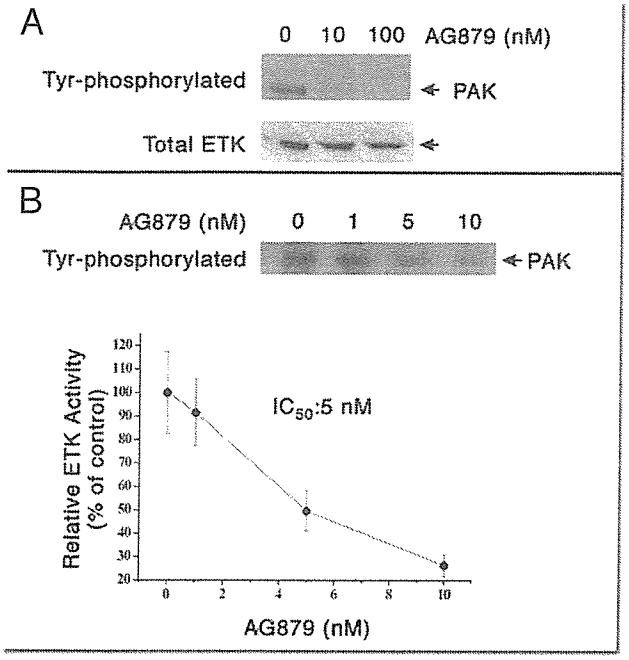

Figure 3. AG879 inhibits the kinase activity of ETK in vitro. The lysates of RAS cells were immuno-precipitated by anti-ETK antibody. The immuno-precipitates (IB) were subjected to an in vitro kinase assay in the presence or absence of AG879 (A, 10 or 100 nM; B, 1 to 10 nM) as described under "Materials & Methods". The ETK activity (Tyr-phosphorylation of PAK1) was monitored by immuno-blot (IB) with anti-PY antibody. Similar protein levels of ETK were detected in all lanes by IB with the anti-ETK antibody. Similar results were obtained from two independent experiments.

immuno-precipitated with the anti-ETK antibody. The immuno-precipitates were subjected to an in vitro kinase assay in the presence or absence of AG879 (0.001–10 μM) as described in the "Materials and Methods". AG879 (10 nM) strongly inhibits the Tyr-phosphorylation of PAK1 by

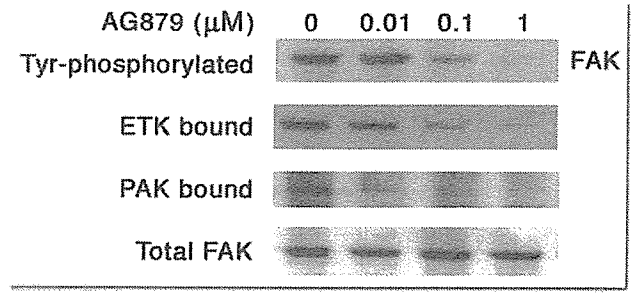

Figure 5. AG879 suppresses the Tyr-phosphorylation of FAK and its association with ETK and PAK1. Serum-starved RAS cells were incubated with AG879 (0.01–1 μM) for 1hr. The cell lysates were immuno-precipitated (IP) with anti-FAK antibody as described under "Materials & Methods", followed by immuno-blot (IB) with anti-phospho-Tyr (PY), anti-ETK or anti-PAK antibodies. Similar protein levels were detected in all lanes by IB with the anti-FAK antibody. Similar results were obtained from two independent experiments.

ETK (Fig.3A), and the IC_{50} for ETK is around 5 nM (Fig. 3B). Furthermore, AG 879 has no direct effect on any other members of TEC family kinases such as TEC, BTK or ITK, even at 10 μM in vitro (data not shown). These results suggest that ETK is so far most sensitive to the action of AG879. However, since the anti-ETK antibody could precipitates not only ETK itself, but also any proteins forming a tight complex with ETK such as PAK1 and FAK, we cannot exclude the possibility that the primary target of AG 879 might be a third Tyr-kinase which is associated with ETK, and responsible for the ETK activation.

AG879 (5 nM) Does Not Inhibit Recombinant ETK from Bacteria or Insect Cells. To clarify whether ETK itself is the primary target of ETK, two different recombinant ETK samples of human origin were purified from bacteria or insect cells: a constitutively activated mutant of ETK called ETKC (residues 243–674) which lacks the N-terminal PH domain purified from bacteria as a GST fusion protein, and full-length ETK purified from insect cells. Either the ETKC or the full-length ETK were not inhibited by AG 879 at 10 nM, although they were significantly inhibited at 1–10 μM (see Fig. 4). Furthermore, in vitro binding of PAK1 in RAS cell lysates to either the PH domain of ETK or a kinase-dead mutant of ETK (called

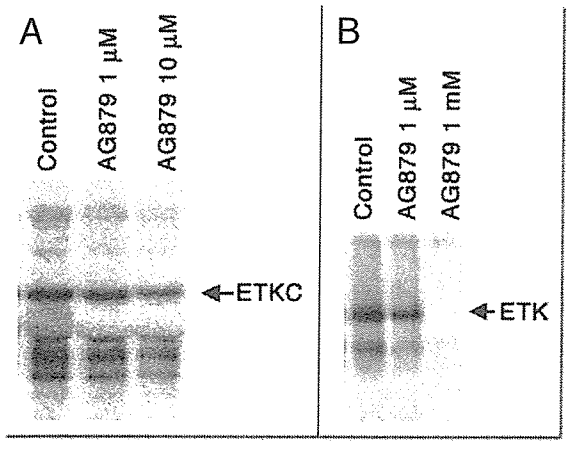

Figure 4. Recombinant ETK proteins alone are far less sensitive to AG 879 in vitro. (A) Effect of AG879 on the ETKC from bacteria. The GST-ETKC was auto-phosphorylated in the presence of AG 879 (0, 1 and 10 μM) in vitro as described under "Materials and Methods". (B) Effect of AG879 on full-length ETK from insect cells. The full-length ETK was auto-phosphorylated in the presence of AG 879 (0, 1 μM and 1mM) in vitro as described under "Materials and Methods".

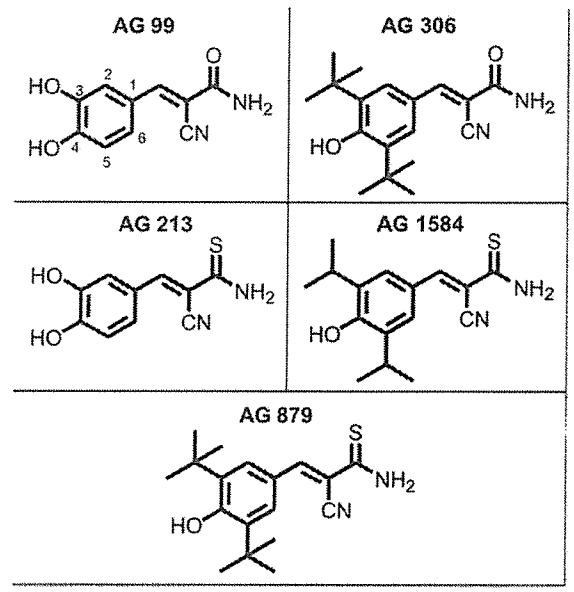

Figure 6. Chemical structure of AG 879 derivatives.

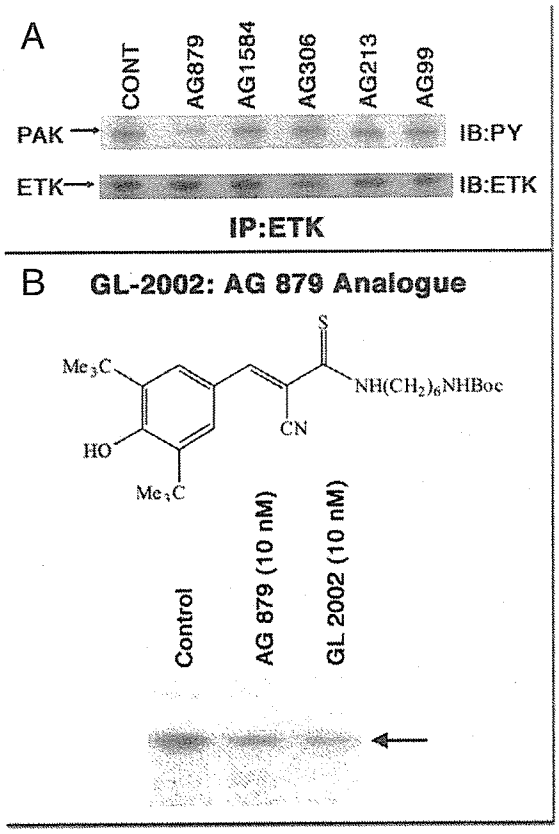

Figure 7. Anti-ETK activity of AG 879 derivatives. (A) The lysates of RAS cells were immuno-precipitated by anti-ETK antibody. The immuno-precipitates (IP) were subjected to an in vitro kinase assay in the absence of any drug (CONT) or presence of either AG879 (10 nM) or four other derivatives (10 μM) as described in Figure 3. Only AG 879 inhibits the ETK activity (Tyr-phosphorylation of PAK1) monitored by immuno-blot (IB) with anti-PY antibody. Similar protein levels of ETK were detected in all lanes by IB with the anti-ETK antibody. Similar results were obtained from two independent experiments. (B) After RAS cells were treated with either 10 nM GL-2002 or AG 879 for 1.5 hrs, each cell lysate was subjected to the in vitro PAK1 kinase assay described in Fig. 1B. GL-2002 strongly inhibited PAK1 activation as did AG 879. Similar results were obtained from three independent experiments.

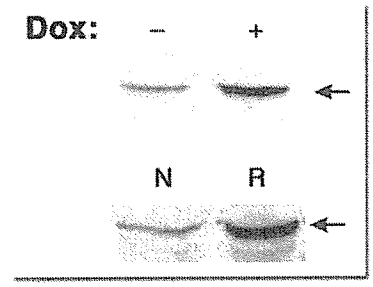

Figure 8. RAS-induced up-regulation of ETK. Upper panel: Up-regulation of ETK by the Doxycyline-induced v-Ha-RAS expression in normal NIH/3T3 cells. Dox-minus, the control (no doxycycline-added); Dox-plus, 2 μg/ml doxycycline added. Lower panel: Enhanced expression of ETK in v-Ha-RAS-transformants. N, normal NIH/3T3 cells; R, v-Ha-RAS-transformants. The arrow indicates the ETK band. Both stable and inducible RAS up-regulate the ETK protein level.

ETK/KQ) as a GST-fusion protein was not inhibited by 10 nM AG879 (Hirokawa Y, He H, Maruta H, unpublished observation, 2002). These observations altogether suggest that the primary target of AG879 is not ETK itself, but rather its associated upstream activator to be identified.

AG879 Inhibits the Tyr-Phosphorylation of FAK and Its Association with ETK and PAK1. ETK is a cytoplasmic (non-receptor) Tyr kinase which is activated at the plasma membranes.[9,10] The N-terminus of FAK shares significant sequence homology with FERM domains, which are involved in linking cytoplasmic proteins to the membranes.[23,24] It was shown recently that the activation of ETK by extracellular matrix (ECM) is regulated by FAK through the interaction between the PH domain of ETK and the FERM domain of FAK, and that activated FAK binds ETK and elevates the Tyr-phosphorylation of ETK.[8]

To test whether the FAK-ETK interaction is affected by AG879, serum-starved RAS cells were treated with AG879 (0.01–1μM). Cell lysates were then immuno-precipitated with anti-FAK antibody, followed by blotting with anti-phospho-Tyr, anti-ETK or anti-PAK1 antibodies separately. As shown in Figure 5, AG879 suppresses both the Tyr-phosphorylation of FAK and its association with ETK at 100 nM, but not at 10 nM, whereas AG879 inhibits the FAK-PAK1 interaction at 10 nM. These results suggest that PAK1 associates with FAK probably through ETK, and PAK1 can no longer interact with FAK when the PAK1-ETK complex is disrupted by AG879.

The Structure-Function Analysis of AG879 Derivatives in Inhibiting ETK. To determine which side chains of AG879 are essential for the ETK inhibition, and further screen for a more potent "ETK inhibitor", we have examined the anti-ETK activity of several AG879 derivatives shown in Figure 6. However, none of these derivatives other than AG879 itself inhibits ETK activity in vitro even at 10 μM (see Fig. 7A). These results indicate that at least both tert butyl groups at positions 3 and 5, and the thio group are absolutely essential for AG879 to inhibit ETK. Interestingly, the ErbB2-specific inhibitor AG825 is distantly related to AG879, but like AG306, lacks both the thio and tert butyl groups, and in fact shows no anti-ETK activity at even 1 μM in vitro (data not shown). However, when the free (thio) amino group of AG879 was alkylated with an amino-hexane chain, the resulting derivative called GL-2002 was still able to show a strong anti-ETK activity that blocks the PAK1 activation in RAS cells even at 10 nM (Fig. 7B), suggesting that, unlike other side chains, this free amino group of AG879 is not essential for its anti-ETK activity. Thus, we are currently generating a series of bioactive immobilized AG 879 (or its water-soluble N-hexylamine derivative, called GL-2003) by coupling them to agarose beads through the amino group so that we can use the AG879/GL-2003 bead as a ligand for fishing a high-affinity AG879-binding protein(s).

Upregulation of ETK Protein Level by RAS. How does RAS activate this integrin/FAK/ETK pathway? Although the whole picture of this mechanism still remains to be unveiled , we found that v-Ha-RAS upregulates the protein level of ETK several folds, using both doxycycline-inducible v-Ha-RAS transformants and stable v-Ha-RAS transformants derived from normal NIH/3T3 cells (see Fig. 8), clearly indicating that oncogenic RAS signalling involves ETK.

DISCUSSION

In this study, we have demonstrated that AG879 selectively inactivates the cytoplasmic Tyr kinase ETK with IC_{50} of about 5 nM. The inactivation of ETK by AG879 blocks the ETK-PAK1 interaction, thereby blocking the Tyr-phosphorylation of PAK1 and its kinase activity. Interestingly at this concentration AG879 does not inhibit directly any other kinases including FAK, PAK, ErbB2, ErbB1, TRK, TEC, BTK and ITK. However, since the IC_{50} of this drug for recombinant ETK proteins alone is 1–10 μM, instead of 5 nM, it is most likely that the primary target of AG879 is not ETK, FAK or ErbB2 themselves, but an as yet unidentified activator of ETK. Thus, we are currently identifying this highly AG879-sensitive